Sequential graft-Interpenetrating polymer networks based on polyurethane and acrylic/ester copolymers

by

Ricardo Ballestero Méndez

A thesis submitted to the Graduate Faculty of
Auburn University
in partial fulfillment of the
requirements for the Degree of
Master of Science

Auburn, Alabama
December 12, 2015

Keywords: thermal properties, graft-IPNs, fracture toughness, BisGMA, sequential polymerization

Approved by

Maria L. Auad, Chair, Associate Professor of Chemical Engineering
Hareesh V. Tippur, Professor of Mechanical Engineering
Gisela Buschle-diller, Professor of Biosystems Engineering
Michael Miller, Professor of Biological Sciences

ABSTRACT

Highly transparent and tough graft-interpenetrating polymer networks (graft-IPNs) were synthesized using an elastomeric polyurethane phase (PU) and a highly stiff acrylate-base copolymer phase. The grafting points between the two networks were generated with the purpose of minimizing the phase separation process of the polymeric systems. In order to generate the grafting between the networks, an acrylic resin capable of undergoing both free radical and poly-addition polymerization was employed. The thermo-mechanical properties, fracture toughness properties as well as network and surface phase morphology of the graft-IPNs synthesized were evaluated in this work. Data obtained suggested that the minimization of the phase separation was achieved by the generation of crosslinking points between both networks. High transparency was obtained in all samples as an indication of the high level of interpenetration achieved. The relative high values obtained for the fracture toughness tests coupled with the high transparency achieved suggest that generating chemical crosslinks between networks is a good approach for diminishing the phase separation process in the systems increasing the compatibility between the networks.

ACKNOWLEDGMENTS

The author would like to express his gratitude to all of those who are a part of his life. I do not dare to write a name since I have come to realize that it is impossible to know the impact that something as simple as a word of kindness would have on the future. I want to also express my gratitude to United States Army Research Office for providing the funds necessary for this research to be conducted through the grant W911NF-12-1-0317.

Table of Contents

ABSTRACT ii
ACKNOWLEDGMENTS iii
Table of Contents iv
List of Tables vii
List of Figures viii
CHAPTER I. 1
INTRODUCTION 1
Transparent Armor 3
Transparent Armor Construction 5
Transparent-armor functional layers 8
Strike-face layer 8
Intermediate layer 9
Spall/backing layer 9
Ballistic Transparent Materials 10
Glass 10
Glass-ceramics 11
Crystalline Ceramics 12
Amorphous Glassy Polymers 13
Multicomponent Polymeric Materials 16
Polymer blend 17
Graft Copolymers 18
Block Copolymers 18
IPNs and semi-IPNs 19

Interpenetrating Polymer Networks 19
Different kinds of IPNs 21
Interpenetrating Polymer Networks used in Transparent Armor Systems 23
Research objective 25
CHAPTER II. 26
Sequential graft-Interpenetrating Polymer networks 26
Introduction 26
MATERIASL AND METHODS 29
Materials 29
Synthesis of graft-IPNs 30
TECHNIQUES 31
RESULTS AND DISCUSSION 36
Analysis of FTIR measurements 36
Thermo-mechanical characterization 39
Network Morphology 45
Degree of transparency 48
Stiffness and fracture toughness 50
Determination of average molecular weight between crosslinks (M_C) and its relation with fracture toughness. 52
Surface Morphology 54
Stress relaxations of graft-IPNs 56
Modeling of Stress Relaxation Behavior of graft-IPNs 60
CONCLUSIONS 65
CHAPTER III. 67
Vinyl ester-based graft-Interpenetrating Polymer Networks 67
INTRODUCTION 67
MATERIALS and METHODS 70

Materials 70
Synthesis of graft-IPNs 71
TECHNIQUES 71
RESULTS AND DISCUSSION 73
Thermo-mechanical characterization 73
Degree of transparency 80
Stiffness and fracture toughness 82
Surface Morphology 85
CONCLUSIONS 88
FUTURE WORK 89
REFERENCES 90

List of Tables

Table 1. Number of casualties during operations OFS, OIR, OND, OIF and OEF, from October 2001-July 2015. 1

Table 2. Individuals with battle-injury major limb amputations for OEF, OFS, OIF, OND and OIR, from October 2001 to June 2015. 2

Table 3. NIJ (0108.01) standard for ballistic-protective materials. 4

Table 4. Determination of extent of reaction at gel point. 39

Table 5. Storage modulus, E´, glass transition temperature, T_g, storage modulus at the rubbery plateau, E_R, and M_C for the different graft-IPNs synthesized. 44

Table 6. Results obtained for the fracture toughness tests performed on different graft-IPNs synthesized. 52

Table 7. Initial stress relaxation modulus of graft-IPNs at different temperatures and copolymer weight percentage. 60

Table 8. Summary of the Stretched exponential and biexponential Maxwell stress relaxation times for graft-IPNs with different copolymer wt%. 61

Table 9. Storage modulus, E´, glass transition temperature, T_g, for the different styrene-based graft-IPNs synthesized. 80

Table 10. Results obtained for the fracture toughness tests performed on different styrene-based graft-IPNs synthesized with 10 wt% of styrene in the copolymer phase. 84

List of Figures

Figure 1. Scheme of traditional transparent armor systems architectures based on glass laminates and polymeric inter-layer, modified from reference [9]. 6

Figure 2. Schematic representation of most recent three-functional-layer design of the transparent-armor systems, modified from reference [9]. 7

Figure 3. Chemical structure of poly(methyl methacrylate) [27] 14

Figure 4. Chemical structure of polycarbonate [28]. 15

Figure 5. Chemical structure of polyurethane [29]. 15

Figure 6. Basic combinations of two polymers: a) polymer blend; b) graft copolymer; c) block copolymer; d) AB-graft copolymer; e) IPN and f) SIPN. Taken from reference [20].....17

Figure 7. Interpenetrating Polymer Network [41]. 20

Figure 8. Synthesis scheme for simultaneous interpenetrating polymer networks.....22

Figure 9. Synthesis scheme for sequential interpenetrating polymer networks.....23

Figure 10. graft-IPNs reaction scheme. 30

Figure 11. FTIR of graft-IPNs at different times during the curing process. 36

Figure 12. Isocyanate conversion plot. 37

Figure 13. DMA results showing change in the storage modulus for graft-IPNs with various ratio of MMA based copolymer to 650 g mol^{-1} PTMG based polyurethane.....40

Figure 14. DMA results showing change in tan δ for graft-IPNs with various ratio of MMA based copolymer to 650 g mol^{-1} PTMG based polyurethane. 42

Figure 15. TEM photos of graft-IPNs with 70 wt% MMA based copolymer using the 650 g mol^{-1} PTMG at (a) 60 °C, (b) 80 °C and 1400 g mol^{-1} (c) 60 °C and (d) 80 °C. 47

Figure 16. UV-vis spectrum of MMA based copolymer and a) 650 g mol^{-1} PTMG based polyurethane and b) 1400 g mol^{-1} PTMG based polyurethane graft-IPN. 49

Figure 17. Stress vs Strain plots for MMA based copolymer samples using (a) 650 g mol^{-1} PTMG and (b) 1400 g mol^{-1} PTMG based polyurethane during tension test.....51

Figure 18. Plot of (a) K_{1c} vs M_C plot and (b) K_{1c} vs $M_C^{1/2}$. 54

Figure 19. SEM photos of (a) 60 wt% copolymer, (b) 70 wt% copolymer, (c) 80 wt% copolymer and (d) 90 wt% copolymer MMA based graft-IPNs samples using the 1400 $gmol^{-1}$ PTMG.....55

Figure 20. Normalized stress relaxation modulus for graft-IPNs with different copolymer content, a) 60%; b) 70%; c) 80%; d) 90%, and e) 100% at three different test temperatures.....59

Figure 21. Fit comparison between the Stretch exponential model and the biexponentail Maxwell model for graft-IPN sample with a copolymer to PU ratio of 90:10.....62

Figure 22. Temperature dependence of τ_s for gaft-IPNs with different copolymer content.....63

Figure 23. Relaxation activation energy, Q_n, as a function of copolymer content. 63

Figure 24. The methacrylation of DGEBA to form vinyl ester monomer, modified from reference [86].....67

Figure 25. Modification of copolymer phase by the addition of styrene.....69

Figure 26. DMA results showing change in the storage modulus for styrene-modified graft-IPNs with various ratio of copolymer to (a) 650 g mol^{-1} PTMG based polyurethane and (b) 1400 g mol^{-1} PTMG based polyurethane. The copolymer was synthesized using 10 wt% of styrene. 75

Figure 27. DMA results showing change in tan δ for graft-IPNs with various ratio of styrene-based copolymer to a) 650 g mol^{-1} PTMG based polyurethane, and b) 1400 g mol^{-1} PTMG based polyurethane 77

Figure 28. DMA results showing change in the storage modulus for styrene-modified graft-IPNs with various amounts of styrene with the 1400 g mol^{-1} PTMG based polyurethane. 78

Figure 29. DMA results showing change in tan δ for graft-IPNs with 1400 g mol^{-1} PTMG based polyurethane and various amount of styrene present in the copolymer. 79

Figure 30. UV-vis spectrum of styrene-based copolymer and 1400 g mol^{-1} PTMG based polyurethane graft-IPN, with increasing amounts of styrene in the copolymer. 81

Figure 31. UV-vis spectrum of styrene-based copolymer and 1400 g mol^{-1} PTMG based polyurethane graft-IPN, with 10 wt% of styrene present in the copolymer. 82

Figure 32. Stress versus Strain plots for styrene-based copolymer samples using (a) 650 g mol^{-1} PTMG and (b) 1400 g mol^{-1} PTMG based polyurethane during tension test. 83

Figure 33. SEM photos of (a) 650 g mol^{-1} PTMG based polyurethane and 10 wt% of styrene, and (b) 1400 g mol^{-1} PTMG based polyurethane and 10 wt% of styrene, (c) 650 g mol^{-1}

PTMG based polyurethane and 45 wt% of styrene, and (d) 1400 g mol^{-1} PTMG based polyurethane and 45 wt% of styrene VE-based graft-IPNs.....87

CHAPTER I.

INTRODUCTION

During the last decade our society has seen a reconfiguration of armed conflicts all over the world. These conflicts are characterized by an escalation in violence and have become more diversified. According to the BBC in their coverage of the Syrian conflict, an estimate of more than 200,000 Syrians have lost their lives in a span of four years of armed conflict, a civil war that is tearing Syria apart [1]. In a recent report done by Fischer H [2] for the Congressional Research Service, shows the statistics regarding U. S. military and civilian casualties as well as major limb amputations in the active missions Operation Freedom's Sentinel (OFS), Operation Inherent Resolve (OIR), Operation New Dawn (OND), Operation Iraqi Freedom (OIF) and Operation Enduring Freedom (OEF) between October, 2001 and July, 2015 are shown in Table 1 and Table 2 respectively.

Table 1. Number of casualties during operations OFS, OIR, OND, OIF and OEF, from October 2001-July 2015, modified from reference [2].

	Deaths (Hostile and Non-Hostile)	Wounded in action
Operation Iraqi Freedom	4,424	31,951
Operation Enduring Freedom	2,355	20,071
Operation New Dawn	66	295
Operation Inherent Resolve	7	1
Operation Freedom's Sentinel	3	33

Table 2. Individuals with battle-injury major limb amputations for OEF, OFS, OIF, OND and OIR, from October 2001 to June 2015, modified from reference [2].

Year	OEF & OFS	OIF, OND, OIR	Total
2001	1	--	1
2002	1	--	1
2003	9	71	80
2004	6	152	158
2005	17	147	164
2006	9	147	156
2007	16	197	213
2008	30	67	97
2009	67	24	91
2010	207	2	209
2011	257	3	260
2012	154	1	155
2013	39	--	39
2014	15	1	16
2015 (partial year)	5	--	5
Total	833	812	1,645

From the results of this report, one can see how critical it is the developing of novel armor systems in order to protect the lives of not only military personal but civilians as well, from the continuing escalations in the number and variety of threats present in today's battlefield.

Transparent Armor

Over the years it has been demonstrated the importance of transparent armor in both military and civilian scenarios. Transparent armor systems are employed in a vast array of critical applications where the situational awareness is the fine line that divides life from death, such as non-combat face-shields for riot control/security personnel, ground/air military/civilian vehicle protection [3]. According to Grujicic and coworkers [4] the implementation of transparent armor for windshields and side-windows in military ground vehicles comprehends the majority of transparent armor systems deployment. In their research they mentioned a set of key functional requirements for transparent armor systems used in ground-vehicle occupant protection, which are mention bellow:

(a) Elevated single and multi-hit blast/ ballistic resistance

(b) Distortion-free and long-lasting surfaces for optical clarity/transparency

(c) Sufficiently low areal density

(d) Small transparent-armor panel-thickness to reduce vehicle interior space claim

(e) Compatibility with the on-board non-visible spectrum imaging and communication equipment

(f) High-wear/low-velocity impact-scratch/damage endurance

(g) High performance-to-cost ratio

As aforementioned, these transparent armors need to be able to withstand high-energy impacts and sustain their optical properties after several impacts. In order to do so, a material needs to meet certain standards against ballistic impacts. The National Institute of Justice (NIJ), which is part of the U. S. Department of Justice, has developed a set of standards to

classify a material's capability to overcome ballistic impacts. The NIJ standards for ballistic-protective materials are shown in Table 3.

Table 3. NIJ (0108.01) standard for ballistic-protective materials, taken from reference [5].

Armor type	Test ammunition	Nominal bullet mass	Suggested barrel length	Required bullet velocity	Required hits per armor test panel	Permitted penetrations
I	22 LHRV	2.6 g	15-16.5 cm	320 ± 12 m/s	5	0
	Lead	40 gr	6-6.5 in	1050 ± 40 ft/s		
	38 Special	10.2 g	15-16.5 cm	259 ± 15 m/s		
	R N lead	158 gr	6-6.5 in	850 ± 50 ft/s		
II-A	357 Magnum	10.2 g	10-12 cm	381 ± 15 m/s	5	0
	JSP	158 gr	4-4.75 in	1250 ± 50 ft/s		
	9 mm	8.0 g	10-12 cm	332 ± 12m/s		
	FMJ	124 gr	4-4.75 in	1090 ± 40 ft/s		
II	357 Magnum	10.2 g	15-16.5 cm	425 ± 15 m/s	5	0
	JSP	158 gr	6-6.5 in	1395 ± 50 ft/s		
	9 mm	8.0 g	10-12 cm	358 ± 12 m/s		
	FMJ	124 gr	4-4.75 in	1175 ± 40 ft/s		
III-A	44 Magnum	15.55 g	14-16 cm	426 ± 15 m/s	5	0
	Lead SWCGC	240 gr	5.5-6.25 in	1400 ± 50 ft/s		
	9 mm	8.0 g	24-26 cm	426 ± 15 m/s		
	FMJ	124 gr	9.5-10.25 in	1400 ± 50 ft/s		
III	7.62 mm	9.7 g	56 cm	838 ± 15 m/s	5	0
	308 Winchester FMJ	150 gr	22 in	2750 ± 50 ft/s		
IV	30-06	10.8 g	56 cm	868 ± 15 m/s	1	0
	AP	166 gr	22 in	2850 ± 50 ft/s		

AP-armor piercing; FMJ-full metal jacket; JSP-jacketed soft point; LRHV-long rifle high velocity; RN-round nose; SWCGC-semi-wadcutter gas checked.

The aforementioned specifications given by the NIJ divide the potential threats into different levels according to projectile parameters such as: type, weight, velocity, barrel length and allowable number of penetrations for a given number of hits per armor test panel. Nevertheless, it is of common knowledge that todays' ballistic threats exceed the ones currently considered in civilian transparent-armor ballistic performance specifications. These protective systems typically cover only protection requirements against handguns and small-caliber rifle rounds, while military vehicles face threats from a broader variety of heavier ammunition. As a result, the US military is currently developing a new transparent-armor test specification standard ATPD 2352 [6]. This new standard highlights all of the new key specifications required for transparent armor systems and it will also serve as a future guide for armor acquisitions by the Army. The ATPD 2352 standard will also specified the ballistic-protection requirements with respect to the standard military threats (bullets of various shapes and calibers), the standard will also contain the ballistic performance requirements with respect to the Fragment Simulating Projectiles (FSPs) as well as the optical transparency properties and environmental durability specification required. The addition of the armor-protection requirements against the FSP threats is of particularly importance taking into account the fact that Improvised Explosives Devices (IED)-related vehicle occupant deaths have been escalating over the years.

Transparent Armor Construction

Traditionally, transparent armor systems are design and constructed as several laminates of glass (soda-lime glass), and adhesive bonded with polymeric layers in between; the most common polymers employed for this purpose are polyurethane and polyvinyl butyral [7]. A schematic representation of the construction of typical transparent armor systems is shown in

Figure 1. As a result of their construction design and the high density of glass, in order to achieve protection against single and multi-hit penetration, several layers of this glass-polymer laminates are needed. This becomes a major disadvantage since it leads to an increase in vehicle weight; reduction in cabin space; increased optical distortions and a reduction of optical clarity/transparency [8].

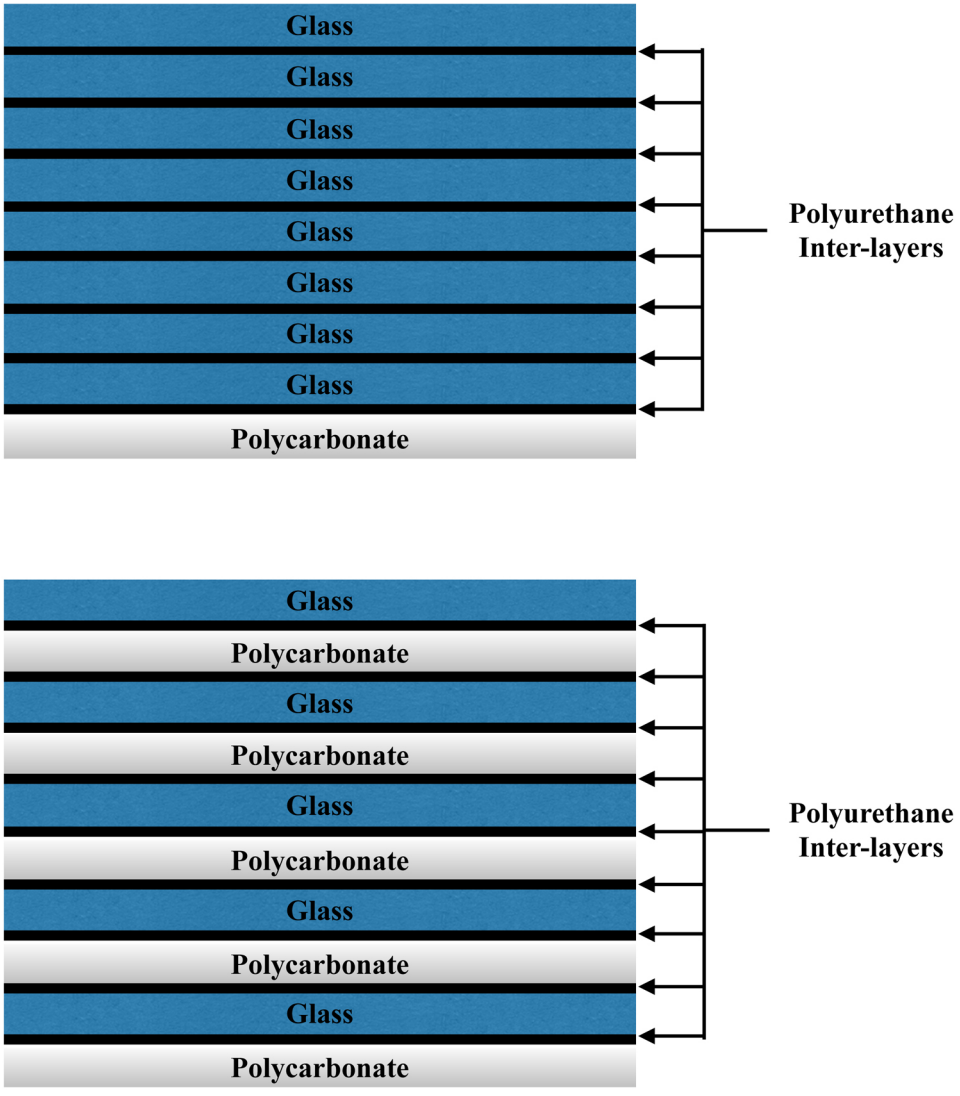

Figure 1. Scheme of traditional transparent armor systems architectures based on glass laminates and polymeric inter-layer, modified from reference [9].

Moreover, in a study conducted by Sands and coworkers [10] they observed how current architecture employed for safety ballistic systems is limited by the mass efficiency. Under this kind of construction the mass of the transparent armor systems contributed as much as 30 % of the overall weight of the armor vehicle, but only offered 15 % of the total covering area of the ground vehicle.

In order to improve the mass efficiency in the transparent armor systems many efforts have been made to improve the architecture of the systems. Most recent transparent armor systems typically consist of three functional layers: a) a projectile-blunting/eroding/fragmenting hard strike face; b) energy-absorbing, crack-arresting, thermal-expansion-mismatch mitigating intermediate layer and c) a fragmented-armor debris containment spall-liner/baking layer [11]. A schematic representation of the aforementioned armor systems can be seen in Figure 2.

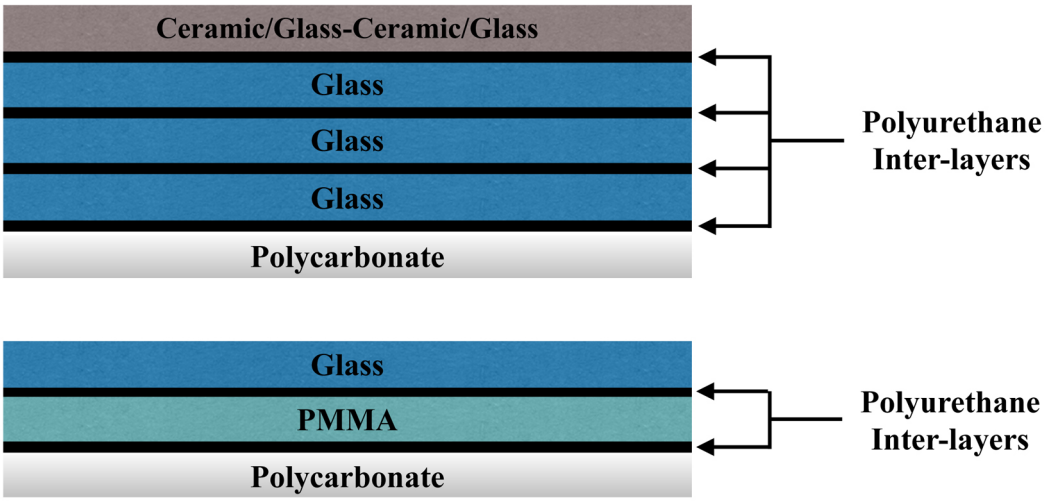

Figure 2. Schematic representation of most recent three-functional-layer design of the transparent-armor systems, modified from reference [9].

Transparent-armor functional layers

As mentioned in the previous section, the most recent architecture in transparent armor systems predominately consists of three different layers. Each of these layers fulfills a critical role in stopping a high-energy impact. The description and requirement for each of these layers is mentioned bellow.

Strike-face layer

The strike-face layer is made from ceramics with high hardness and mechanical properties in order to decelerate the projectile and to dissipate its impact energy. As ceramics are inherently brittle, their inner constituents show extensive cracks after receiving an impact from a first projectile at high velocity. Such damage weakens the armor panel, and so has adverse effect on penetration of a following projectile, impacting within a few centimeter of the first [12]. The functional requirements for this layer are summarized as follows:

a) High optical transparency in the visible and infrared wavelength ranges.

b) High ability to blunt projectile through prolonged interfacial dwelling and mechanical erosion.

c) Good low-velocity (stones, pebble, etc.) impact damage resistance.

d) Good environmental resistance (thermal gradients, sand erosion, ultra violet radiation, etc.)

Intermediate layer

In this layer, since the projectile has already been slowed down (and consequently, fragment accelerations are lower), the effect of its erosion becomes secondary to the energy-absorption accompanying fracture of the resistance layer material. This layer requires high bending strength and bending recovery to increase the resistance of the former layer [13]. The functional requirements for this layer are summarized as follows:

a) High optical transparency in the visible and infrared wavelength ranges.

b) High kinetic energy absorption capability via fine-scale fracture/fragmentation.

c) High bending stiffness in order to provide stiff backing support to the strike-face layer.

d) The ability to localize cracking/damage in order to not compromise in the armor's multi-hit ballistic performance.

e) Good environmental resistance (thermal gradients, ultra violet radiation, etc.).

Spall/backing layer

The role of the backing layer is to provide support for the intermediate layer in order to avoid surpassing its bending strength under the projectile impacting [14]. The functional requirements for this layer are summarized as follows:

a) High optical transparency in the visible and infrared wavelength ranges.

b) Projectile/armor spall containment capability.

c) Good environmental resistance (thermal gradients, sand erosion, ultra violet radiation, etc).

d) High chemical/chemical-warfare-agent resistance.

e) High resistance to scratching, etc.

Ballistic Transparent Materials

Traditionally the most common materials for the construction of transparent armor applications are: a) glass (soda-lime glass); b) devitrified glass ceramics; c) mono-crystalline and sub-micron grain size polycrystalline ceramics; and d) thermoplastic and thermosetting amorphous glassy polymers [15]. In this section a brief overview of the most important functional and processing attributes of each of the aforementioned materials is provided.

Glass

For many years, soda-lime glass (also known as float glass) it has been used in transparent armor applications because of its good combination of properties like stiffness, compressive strength and durability. Furthermore, glass-structure fabrication technologies enable the production of curved, large surfaces, transparent structures with thickness approaching several inches, relatively low material and manufacturing costs and controlled crystallization, improving the shock/ballistic impact survivability of the transparent structure. Because of all of these attributes ballistic glass remains as an important constituent material in the majority of transparent impact-resistant systems used today [16]. However, glass-based transparent armors are generally heavy due to their large areal density. Many efforts have been made to

try to reduce the areal density of ballistic glass. Recently, Shim and coworkers [17] evaluated the areal density of a strengthened soda-lime silicate (SLS) glass as a function of areal density. In their study they were able to improve some critical properties like the fracture toughness and flexural strength by 5% and 250%, respectively while decreasing the areal density from 68.85 to 50.06 Kg/m^2.

Glass-ceramics

Glass-ceramics were discovered in 1953 by Stanley Stookey while working for Corning Glass Works, and ever since a lot of research has been done on the material. Glass-ceramics also known as vitrocerams, are produced by controlled crystallization of certain glasses. Glass-ceramics are inherently free from porosity, which in principle gives them several advantages such as: a) the can be mass produced by any glass-forming technique; b) it is possible to tailor their nanostructure for a given application; c) as previously mentioned, they present zero or very low porosity and d) it is possible for the material to combine a variety of desired characteristics. These materials display values on average of fracture strength between 100-250 MPa and fracture toughness between 1-2.5 MPa $m^{1/2}$, which are higher than those of most commercial glasses. However, most glass-ceramics present lower hardness and Young's modulus than ceramics, but present the great advantage of lower areal density and a much lower production cost [18].

Crystalline Ceramics

Crystalline ceramics are primarily used as the strike-face layer in some of the most advanced transparent armor systems today, due to their exceptional hardness/compressive strength properties. Among this branch of materials, three groups are generally considered: a) single crystal transparent ceramics such as Al_2O_3-based sapphire; b) sub-micron grain size polycrystalline transparent ceramics like aluminum-oxy-nitride (ALON^{TM}) and c) magnesium-aluminate Spinel fine-grain transparent ceramics. A brief description of the aforementioned materials is given in bellow.

Sapphire

The single crystal form of pure aluminum oxide (Al_2O_3) or sapphire has a hexagonal-scalenohedral crystal structure with an anisotropic material behavior that is highly dependent on crystal orientation. Due to its excellent mechanical properties, optical transparency, infrared (IR) transmission and commercial availability, sapphire has emerged as a promising high-performance transparent material. Sapphire when compared to glass, offers improved durability, reduced weight and increased protection in a range of harsh-environment applications like bullet-resistance armor windows. Strictly from the transparent armor applications point of view, de most desirable characteristics offered by sapphire are: a) high stiffness and hardness/compressive strength; b) intermediate density; c) high chemical resistance and d) wide availability. However, the maximum panel sizes are very limited and sapphire has a high cost primarily because of expensive machining and polishing processes [19, 20].

ALON™

Transparent aluminum oxynitride (ALON™) ceramics have attracted more attention as a ceramic material for IR/visible windows, transparent armor systems, and several other applications due to its excellent mechanical properties. When compared to single crystal sapphire, aluminum oxynitride ceramics like ALON can be formed into near-net shapes, save energy and greatly reduce the machining costs. ALON ceramics are considered to match or even outperform sapphire with respect to most of the structural/environmental properties [21, 22]. However, to date it is a challenge to manufacture ALON ceramics with an in-line transmittance above 80% as explained by Su and coworker [23].

Spinel

Magnesium aluminate spinel ($MgAl_2O_4$), commonly known as Spinel, is a translucent ceramic that is developed by Westinghouse. This material has attracted a lot of attention for its application in transparent armor systems due to its excellent mechanical properties and relatively high IR cut-off wavelength [24]. Nonetheless, according to Kim and coworkers [24], the fabrication of large $MgAl_2O_4$ with transmittance above 80 % is still a big challenge.

Amorphous Glassy Polymers

Amorphous glassy polymers are generally used as the intermediate or spall/backing layer in most recent transparent armor systems, due to the ductility that this kind of materials present. Currently, poly(methyl methacrylate), PMMA, and polycarbonate, PC, along with polyurethane, PU, are the most frequently found polymers for transparent armor applications [25]. A brief description of these polymers and their properties is given bellow.

Poly(methyl methacrylate), (PMMA)

It is believed that the capability of PMMA to absorb energy from a ballistic impact by a deformation mechanism is a result of its ductility. Patel and coworkers [26], describe how PMMA's ductility is related to the molecular relaxation of the side chain carbonyl ester groups present in its chemical structure, see Figure 3. The molecular mobility of these side chain groups is rather flexible at ambient temperatures, nonetheless, these short side groups become utterly immobilized once they are exposed to conditions in which the rate of mechanical deformation increases and reaches a threshold value. Some of the most valuable characteristics of PMMA for transparent armor systems are: a) relatively high elastic stiffness; b) ultra violet radiation resistance; c) chemical resistance; d) scratch resistance and e) high optical transparency.

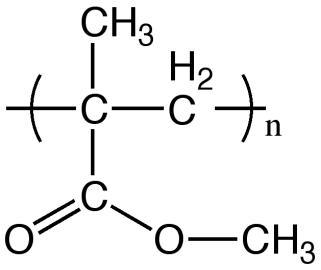

Figure 3. Chemical structure of poly(methyl methacrylate) [27]

Polycarbonate

It is well known that polycarbonate has superior fracture toughness to that of PMMA; as a result, PC is more frequently used in transparent armor systems as the spall/backing layer. The ductility shown by PC is attributed to the molecular motions in its main chain, see Figure 4. These motions are thought to be present even upon exposure to high-rate mechanical

deformations, which gives PC its efficiency in dissipating the energy coming from a ballistic impact [26].

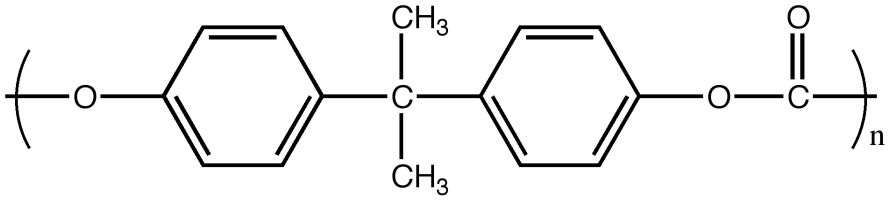

Figure 4. Chemical structure of polycarbonate [28].

Polyurethane

Polyurethane is a highly desirable material for engineering applications due to its inherent molecular microstructure, see Figure 5. Furthermore, the possibility of modifying its chemical structure to obtain glassy like materials or soft and flexible like elastomers makes it a really practical material for its application in armor systems. However, most available polyurethanes present a slight tinting, which affects the optical transparency in thicker sections. For this reason polyurethanes are mostly used as a thin-film adhesive interlayer in transparent armor systems [4].

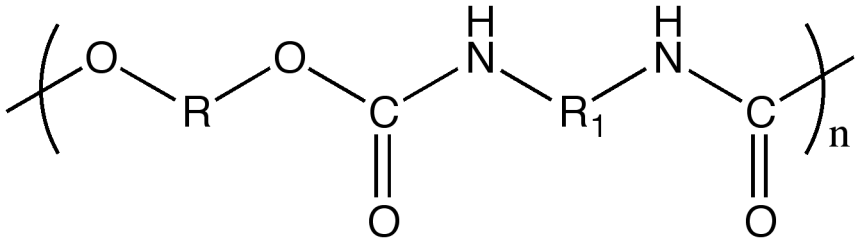

Figure 5. Chemical structure of polyurethane [29].

As it was mentioned before, the approach of using a multilayer architecture for the construction of transparent armor systems generally results in a very high areal density in order to achieve the desired level of protection. This excess in weight not only affects negatively the vehicle's fuel economy but also their transportability, deployability and mobility. The added weight also increases the probability of mechanical and structural failure in the battlefield. Therefore, an increasing number of research groups all around the world have been devoted to the development and design of light-weight, low cost transparent armor materials with superior ballistic penetration performance as well as blast survivability. Among the novel most recent approaches aimed to increase the mass efficiency of transparent armor systems, the development and used of different polymeric materials has attracted a lot of attention. The choice of polymeric materials for such applications is due to their relative low density when compare to other high-performance materials, as well as for the capability that polymers offer to tailor their properties according to the present needs. In the following section, a literature review of the different polymer blends used in high-performance engineering applications is given.

Multicomponent Polymeric Materials

When two or more polymeric materials are mixed, the composition obtained as a result of the mix can be called a multicomponent polymeric material. There are many different ways, in which two different kinds of polymers can be mixed, see Figure 7. The result of mixing different polymers in an extruder gives a polymer blend. If the different chains are bonded together the result can be a graft copolymer (there is bonding between some portion of the backbone of polymer I and the end of polymer II), or a block copolymer (where chains are bonded end to end). Some other types of copolymer are AB-crosslinked copolymers (here

two polymers make up one network), and the interpenetrating polymer networks, IPNs, as well as semi-interpenetrating polymer networks, SIPNs [30]. Further description of the different polymer blends is given bellow.

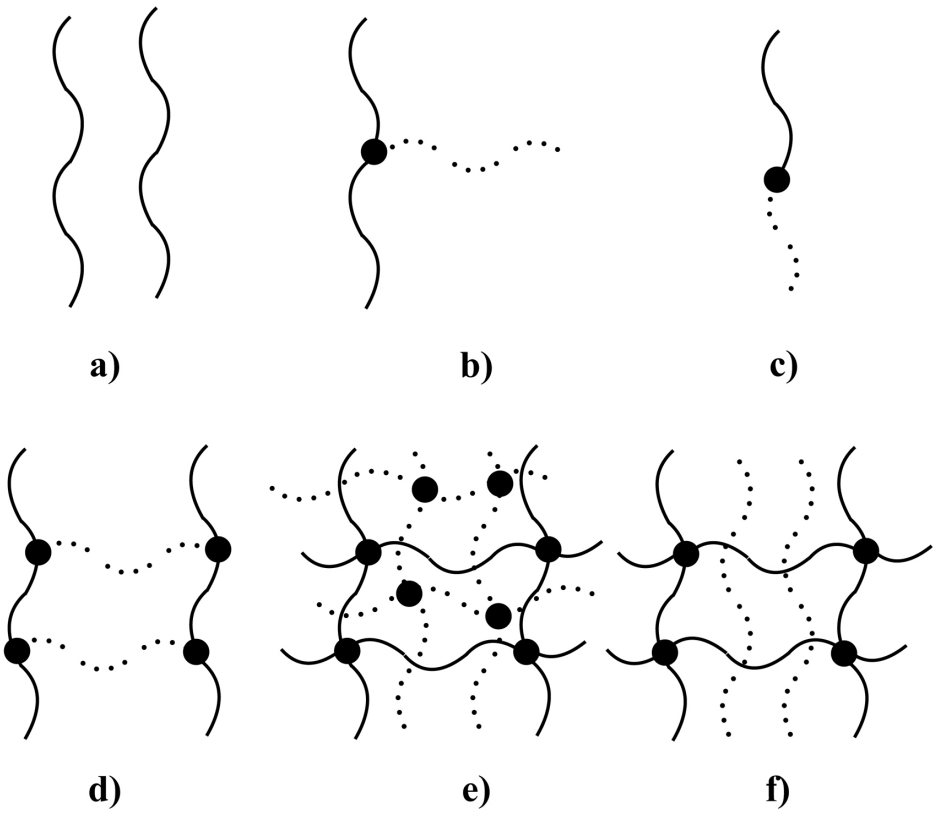

Figure 6. Basic combinations of two polymers: a) polymer blend; b) graft copolymer; c) block copolymer; d) AB-graft copolymer; e) IPN and f) SIPN. Taken from reference [20].

Polymer blend

In most scenarios, neat polymers are not able to provide all the required properties for high-performance engineering applications such as toughness, strength, environmental resistance, etc. Thus, they are usually combined with one or more other polymers in order to fulfill the desired requirements [32]. Polycarbonate is a widely used polymer in transparent ballistic resistant armor systems; nonetheless, polycarbonate may brake in a brittle manner at low

temperatures. In order to overcome this problem many researchers have try to solve this problem by blending polycarbonate with another polymeric material. In a study conducted by Sivaraman and coworkers [33] they describe the use of a polycarbonate/thermoplastic blend to improve the impact strength sensitivity and thickness as well as to improve solvent resistance of neat polycarbonate.

Graft Copolymers

Many different high-performance polymeric materials have been synthesized by means of macromolecules with a wide variety of architectures containing hard backbone and soft branches (grafts). The generation of grafts in a copolymer is generally done with the intention to improve the miscibility and processing of this kind of polymer blend. As a result of the improvement in miscibility, most graft copolymer also exhibited an improvement in their mechanical properties [34]. Jouenne and coworkers [35] mentioned how in order to improve polystyrene's (PS) toughness a graft copolymer of polystyrene and polybutadiene (PB) was developed. Here, the improvement in toughness was achieved by controlling the dispersion of the micro-size particles of polybutadiene thanks to the formation of PS homopolymer chains as well as PB-g-Ps graft copolymers, resulting in a multiphase material.

Block Copolymers

This kind of polymer multiphase system belongs to a special category of self-assembled nanostructurated materials. Block copolymers present the ability of controlling their structure, size and morphology by modifying their molecular structure, molecular weight and

composition. This versatility has attracted a lot of attention from the scientist community as well as the industry for their potential application in high-performance materials [36]. LaShonda and co-workers [37] described the use of a new poly(arylene ether sulfone), PAES, and polydimethylsiloxane, PDMS, and bisphenol A, BA, block copolymers to improve the optical and mechanical properties of the final material, when compared to its parent constituents.

IPNs and semi-IPNs

In the past five decades, interpenetrating polymer networks have attracted the attention of the scientific community. This is due to the possibilities of achieving materials with excellent physical properties such as high-toughness, optical transparency and excellent damping behavior [38]. Both IPNs and semi-IPNs belong to a category of polymeric materials known as multicomponent polymers or polymer alloys. Moreover, these kinds of polymers are prepared by chemical means, such as crosslinking, with the idea of improving the compatibility of otherwise immiscible polymer blends [39]. A broader description of interpenetrating polymer networks is given in the following section.

Interpenetrating Polymer Networks

Sperling L. H [40] defines an interpenetrating polymer network as the combination of two or more other polymers in network form that are synthesized in juxtaposition, see Figure 7.

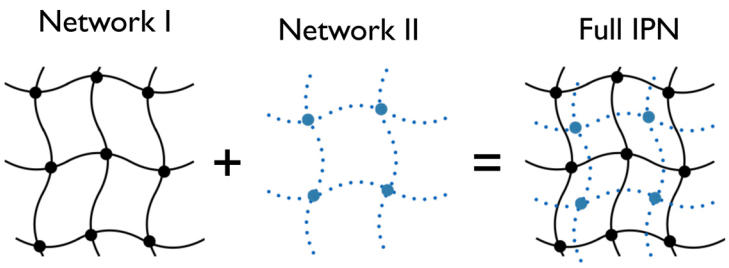

Figure 7. Interpenetrating Polymer Network [41].

It is generally known that the vast majority of IPNs do not interpenetrate at the molecular level, but rather form different phases finely divide at the nanometer scale. This phase separation shown by interpenetrating polymer networks is a complex subject both theoretically and experimentally.

Nevertheless, these kind of multicomponent polymeric systems represent an excellent approach for combining the properties of different polymeric materials in a synergetic way. This kind of behavior was described by Li and co-worker [42] in their study on force compatibility. They found that even though there exist phase separation in IPNs, these materials usually presented highly uniform phase structures, much better than those of the parent polymer blends. They attributed this behavior to the particular network structure of IPNs. Where the higher compatibility achieved could be called “force compatibility”, since the mixing enthalpy does not play a major role in the improvement of miscibility of the system.

Different kinds of IPNs

Over the years IPNs have been classified into many different ways. One way is to divide them into a full-IPNs in which all networks are crosslinked and into semi-IPNs, in which one or more polymers are crosslinked and one or more are linear or branched [43].

Latex interpenetrating polymer networks, LIPNs, are another kind of IPN that is prepared by multistage emulsion polymerization, generally presenting a core and shell structure. LIPNs have been broadly used in the synthesis of rubbers, plastic modification, coatings, adhesives, damping materials, as well as in medical materials [44]. Shi and co-workers [45] investigated how to control the morphology of these LIPNs by means of controlling the particle growth of the system for its potential application on the biomedical field.

Gradient interpenetrating polymer networks are another kind of IPNs. These are materials in which the overall composition or crosslink density of the material varies from location to location at the microscopic level [40]. Lipatov and co-worker [46] how a gradient IPN can be seen as stack of layers of polymer blend with the composition and physical properties gradually changing from surface to the center of the material. In a study carried out by Berry and co-workers [47] a series of poly(ether urethane) with urea and acrylamide. They were capable of synthesized high-strength water absorbing hydrogels offering good biocompatibility for medical applications.

IPNs can also be classified according to their synthesis method as Simultaneous IPNs (SIN) and as Sequential IPNs. During the simultaneous synthesis, the monomers or polymer constituents, plus crosslink agents and catalyzers are mixed together. And then the reaction is carried out simultaneously as indicated by its name, but there is no interference whatsoever between reactions, see Figure 8 [48, 49].

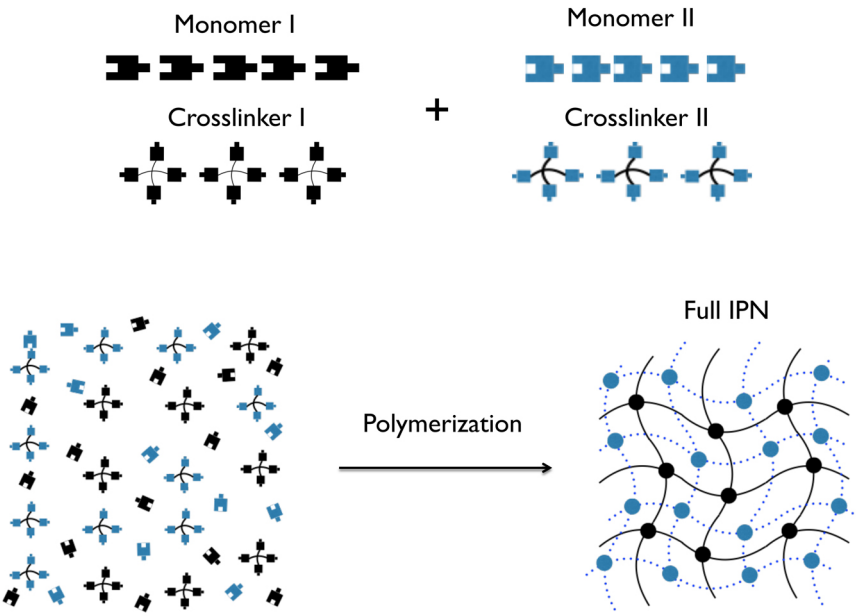

Figure 8. Synthesis scheme for simultaneous interpenetrating polymer networks.

In the case of sequential method, polymer network I is synthesized first and then monomer II plus crosslinking agents and catalyzers are swollen into the network I and polymerize in situ, see Figure 9. As in the case of the simultaneous synthesis method, the two polymerization reactions are carried out without any interference [40, 50].

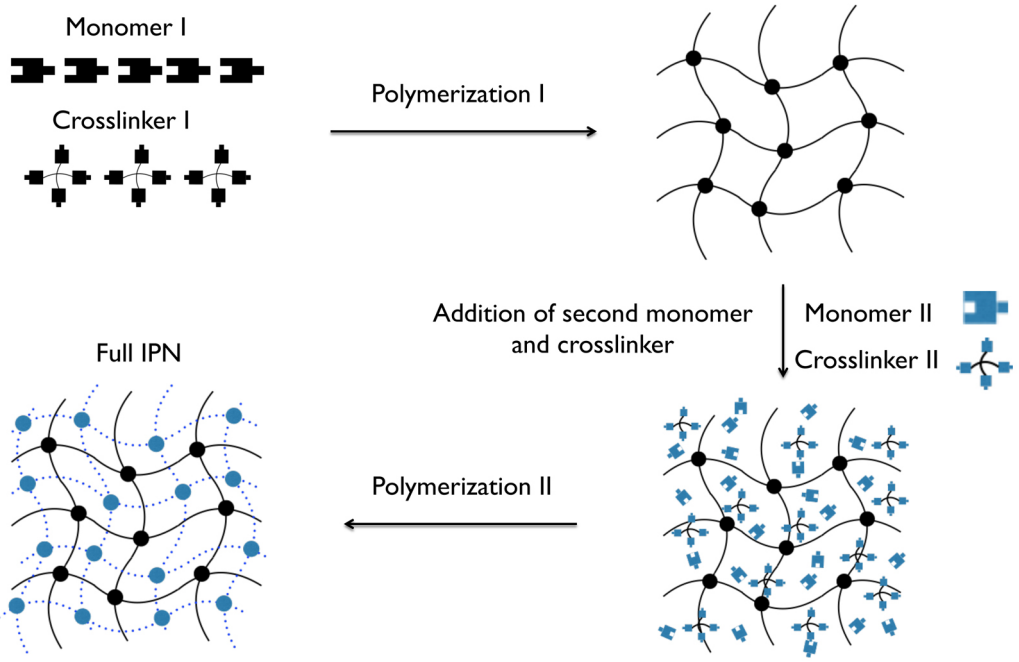

Figure 9. Synthesis scheme for sequential interpenetrating polymer networks.

Interpenetrating Polymer Networks used in Transparent Armor Systems

As it has been discussed in previous sections, in order to improve a vast variety of military and civilian structures and vehicles against blast and ballistic threats, there has been a great interest in developing and deploy novel impact resistant transparent materials. These materials need to present lower densities to maximize mobility and reduce wear as a consequence of the added weight. They also need to present high optical transparency.

Currently available materials for transparent armor applications are limited to a small number of polymers, glasses and ceramics. For this reason, a lot of researchers around the world have approach this problem by producing different multicomponent polymeric systems in order to improve current materials and to adapt to the escalation and diversification of today's threats. As aforementioned, polycarbonate is a ductile thermoplastic, which is widely used for

transparent armor materials. Nonetheless, it is limited by its notch sensitivity in thicker samples and by its processing properties. Several efforts have been made to improve the mechanical properties of polycarbonate. Yin and co-workers [51] described how using small amounts of acrylonitrile-butadiene-styrene (ABS) in an alloy of PC/ABS had significantly reduced polycarbonate's notch sensitivity and improved its processing properties. Following this line of thought, other research groups have tried to toughen transparent epoxy resins by the addition of rubber and rigid particles. An example of this is the study carried out by Gao and co-workers [52], where a rubbery block copolymer grafted SiO_2 toughened epoxy was synthesized. By this method, they were able to improve the fracture toughness as well as the fracture energy.

Bird and co-workers [53] however, followed a different approach to solve this problem. In their work, a full-IPN of polyurethane and poly(methyl methacrylate) was synthesized. In this case, the polyurethane was the soft, rubbery high-impact absorbing phase, while the highly stiff PMMA provide strength and high modulus to the system. By following this approach, they were able to improve the fracture toughness of neat PMMA by 70 %, while keeping an optical transparency above 80 %. Nonetheless, they found that depending on the length of the diol employed for the synthesis of the polyurethane network, phase separation was obtained, losing some of the optical transparency.

Research objective

The purpose of this research is to address the phase separation problem of full-IPNs by generating chemical crosslink points between networks, thus, generating a class of IPNs called graft-IPNs. The graft-IPNs synthesized in this work consisted of a highly stiff copolymer phase, which is comprised of the bis(2-hydroxy-3-methacryloxypropyl) ether (BisGMA) resin and three different monomers capable of radical polymerization: methyl methacrylate (MMA), triethylene glycol dimethacrylate (TEDGMA), and styrene; and a soft based on a rubbery polyurethane phase (PU) with a high flexibility and capability of energy absorption. The crosslinking of the two networks is accomplished by means of the BisGMA resin. This resin has terminal double bonds and secondary hydroxyl groups, which allows the resin to react with the acrylic monomers by radical polymerization, as well as undergo a polyaddition between the secondary (-OH) groups and the (NCO) groups of the isocyanate. In this work, it is hypothesized that the generation of crosslinks points between networks could minimize the phase separation and at the same time improve the mechanical properties of the final material. In this work we also studied the influence that the different PU and copolymer constituents have on the physical properties of graft-IPNs was studied.

CHAPTER II.

Sequential graft-Interpenetrating Polymer networks

Introduction

Over the past decades, polymer blends also known as multiphase polymeric systems have been employed in a broad number of design applications that require high resistance to fracture, a highly desired characteristic for virtually all engineering materials [54]. These polymeric materials became appealing due to their low density when compare with other engineering materials, due to the ability to synergistically incorporate properties of their individual components and achieve materials with better mechanical properties than the original constituents, as well as for their transparency [55].

The challenges with these multiphase systems are to improve their compatibility and interfacial adhesion between phases, so as to guarantee the desired performance of the final material. It is known that only a relative small number of polymer pairs form miscible blends, mostly because of these blends have low entropy of mixing. Although the entropy of mixing favors the miscibility of a given system, it also depends on the number of molecules per unit volume. Thus, the higher the molecular weight of the polymers involved, the fewer molecules per unit volume and the lower the entropy of mixing. And since the heat of mixing of

polymers pairs is generally unfavorable, polymer blends tend to macroscopically phase separate, leading to systems with poor mechanical properties [56, 57, 58].

In order to overcome this problem, many efforts have been made to find different ways to improve the miscibility of multiphase systems, one of this approaches involves the use of interfacial agents. These agents decrease the average domain size of the disperse phase by acting as steric barriers at the interphase region, enhancing the level of interactions between the polymer phases [59, 60, 61].

Another well-known method to minimize phase separation in a polymeric system is through interpenetrating polymer networks (IPNs). Mignard and coworkers [58] define an interpenetrating polymer network as a system constituted by two or more polymer networks partially interlaced on a polymeric scale but not chemically crosslinked. Different kinds of IPNs can be found based on the synthesis method; the two most common methods for their synthesis are sequential and simultaneous polymerization [58]. In the synthesis of IPNs, at least one of the polymers in the system is in the form of a monomer, and since most monomers are small molecules they have appreciable entropy of mixing. Also, the presence of physical interlocks give to the IPNs a more uniform phase structure than those of the parent polymer blends, leading to what is called force miscibility, since the compatibility is not achieved by the mixing enthalpy or entropy [42, 58].

Nevertheless, IPNs usually present some degree of phase separation at some stage of the synthesis. For instance, it has been observed that synthesis of IPNs by simultaneous method

results in phase separation [62]. Phase separation in sequential polymerization has also been observed, here, the entropy of mixing is lost during the second polymerization, due to the increase in size of the molecules as the polymerization continues [57].

In early works done by C. Chen and coworkers [63] and L. Hua and coworkers [64] they reported the implementation of a vinyl ester resin (VE) with a polyurethane network for the synthesis of simultaneous interpenetrating polymer networks. This VE resin was capable of undergoing both free radical polymerization as well as step-wise polymerization. Here the formation of crosslinks between networks was never the objective. Furthermore, the generation of crosslinks was in fact avoided. Studies on the morphology showed clearly that more that one phase was present in the system, as a result of the phase separation between networks.

In the present work, we addressed the phase separation problem of IPNs by generating chemical crosslink points between two networks, thus, generating a class of IPNs called graft-IPNs. Furthermore, the time dependent properties of these novel graft-IPNs are also studied in order to characterize the stress relaxation displayed by our system. The synthesis of graft-IPNs was carried out using the sequential methodology, where the PU phase was polymerized first. Then the copolymer, which was swelling the elastomeric phase, was polymerized in situ within the PU network. The thermo-mechanical properties, fracture properties, stress relaxation properties as well as the phase morphology of the graft-IPNs were studied in this work.

MATERIASL AND METHODS

Materials

For the synthesis of the polyurethane phase (PU), two polyols were employed: 2-ethyl-2-(hydroxymethyl)-1,3propanediol (TRIOL) from Acros Organics, (USA), and poly(tetramethylene ether) glycol (PTMG) average M_n ~ 650 and ~1400 g mol^{-1} from Sigma-Aldrich, (USA). Both TRIOL and PTMG were mixed beforehand, through melting. The TRIOL and PTMG mixture was melted in an oven under strong vacuum to remove moisture. This procedure was employed for the different molecular weight PTMGs. The isocyanate used was hexamethylene diisocyanate 98.0% (DCH) from TCI, (USA). Two catalysts were used for the synthesis: dibutylin dilaurate, 98% (DD) distributed by Pfaltz & Bauer, (USA) and triphenylbismuth, 99+% (TB) from Alfa Aesar, (USA). Ethyl acetate was used as an analogue for both catalyzers.

The copolymer was synthetized using the bisphenol A bis(2-hydroxy-3-methacryloxypropyl) ether (BisGMA) from Esstech, (USA) and two acrylic monomers: methyl methacrylate 99% stabilized (MMA) from Alfa Aesar, (USA) or triethylene glycol dimethacrylate stabilized (TEGDMA) from TCI, (USA) (see Structure 1) while 2,2'-azobis(2-methylpropionitrile), 98% (AIBN) from Sigma-Aldrich, (USA) was used as an initiator.

Synthesis of graft-IPNs

The synthesis of the different graft-IPN systems, see Figure 10, was carried out in a single-step procedure. Both the copolymer phase and the PU phase were prepared separately at room temperature conditions.

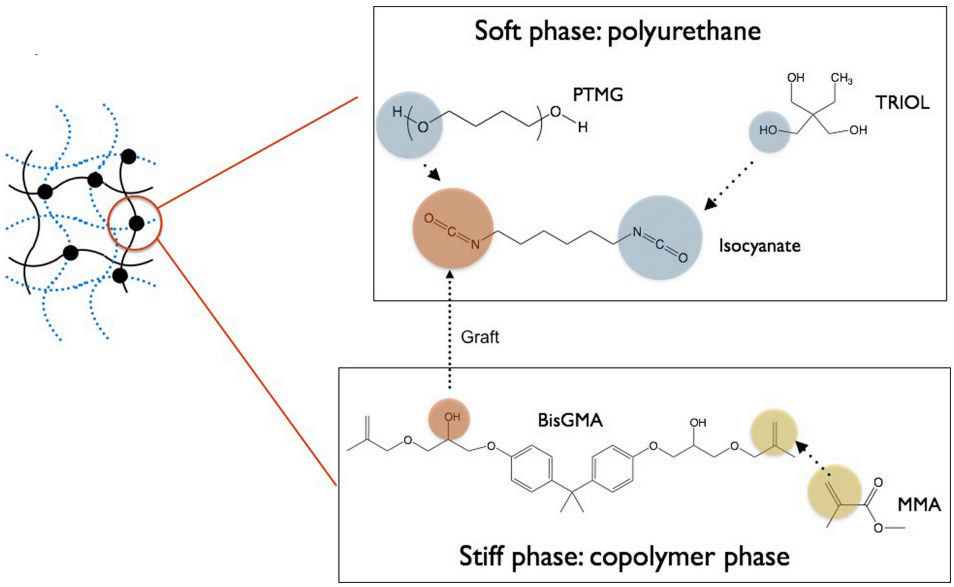

Figure 10. graft-IPNs reaction scheme.

First, the copolymer was prepared by mixing the acrylic monomer (MMA or TEGDMA) with the BisGMA resin, keeping a mass ratio of 90:10 acrylate:BisGMA. The amount of radical initiator employed for the polymerization was 1 wt% of the total copolymer mass. For the polyurethane phase, the DCH was added to the PTMG/TRIOL mixture. The following ratio was used to synthesize all polyurethane networks, 0.19eq TRIOL: 0.12eq PTMG: 0.31eq DCH. In order to generate the crosslink points between networks, an additional quantity of DCH was added to the polyurethane precursor solution in a eq ration of 1:1 DCH:BisGMA. Then, the polyurethane precursors were added to the copolymer precursor solution. Following this, DD and TB were added to catalyze the polyurethane system. After mixing

both solutions, all samples were placed in an oven at 40°C for 17 h after which the samples were transferred to a water bath where the temperature was raised to 60°C for 24 h and finally the temperature was raised to 80°C for 24 h.

Several graft-IPN formulations were prepared following the above-mentioned procedure. The ratio of copolymer to polyurethane content changed from 90 wt% copolymer and 10 wt% PU to 50 wt% copolymer and 50 wt% PU, this was reproduced for the 650 and 1400 g mol^{-1} PTMG methyl methacrylate based graft-IPNs, as well as for the 650 g mol^{-1} PTMG triethylene glycol dimethacrylate based graft-IPNs.

TECHNIQUES

Fourier Transform Infrared (FTIR)

Fourier transform infrared spectroscopy was done using a Thermo Scientific Nicolet^{TM} 6700 spectrometer in attenuated total reflection (ATR) infrared mode. The analysis was carried out within the frequency range of 4000-400 cm^{-1} by co-adding 32 scans and at a resolution of 2 cm^{-1}.

Extent of Reaction at Gel Point

The extent of reaction at the gel point was determined by Flory and Stockmayer's statistical approach to gelation.

Dynamic Mechanical Analysis

Dynamic mechanical analysis (DMA) on a TA Instruments RSA III was carried out to assess the thermo-mechanical properties by three-point bending. The tests were performed at temperatures ranging from -45 to 200 °C with a heating rate of 5 °C/min. The frequency was fixed a 1Hz and a sinusoidal strain-amplitude of 0.1 % was used for the analysis. The dynamic storage modulus (E′) and tan δ curves were plotted as a function of temperature. The temperature at the maximum in the tan δ curve was taken as the T_g. The E´ at T_g + 50 °C was chosen as the rubbery plateau modulus, E_R, for each system.

Molecular Weight between Crosslinks

The average molecular weight between crosslinks (M_C) for the 650 and 1400 g mol^{-1} PU based systems was calculated using Equation (1), which is based on the theory of rubbery elasticity [68].

$$M_C = \frac{3\rho RT}{E_R} \quad (1)$$

Where ρ is the density of the sample; T is the temperature (K); R is the universal gas constant, and E_R is the storage modulus in the rubbery plateau at temperature T.

Transmission Electron Microscopy

Transmission electron microscopy (TEM) on a Zeiss EM 10C 10CR microscope was used to study the morphology of the different networks. Samples were prepared using Kato's osmium tetroxide (OsO_4) staining method, as described elsewhere [53]. All samples were stained for 48 hours prior to analysis.

Ultra violet Spectroscopy

UV- Vis transmittance spectra was collected for the various ratio of MMA based copolymer to 650 and 1400 g mol^{-1} PTMG based polyurethane. A UV-Vis 2450 spectrophotometer from Shimadzu Scientific Instruments was employed to acquire the spectra data. All samples were analyzed in the 900-400 nm range.

Scanning Electron Microscopy

Scanning electron microscopy (SEM) on a Zeiss EVO 50 variable pressure scanning electron microscope with digital imaging and EDS (were the graft-IPNs were sputter coated with an EMS 550X auto sputter coating device with carbon coating attachment) was used to study the fracture surfaces of the 1400 g mol^{-1} PTMG based system.

Fracture Toughness

In order to characterize the fracture toughness of the graft-IPNs synthesized, in terms of the critical stress intensity factor, K_{IC}, quasi-static fracture tests were performed. The cured graft-IPN sheets were machined into rectangular coupons of dimensions 70 mm x 20 mm and 2.8 mm thickness in case of 650 g mol^{-1} PTMG methyl methacrylate based graft-IPNs and 70 mm x 15 mm and 2.8 mm thickness for 1400 g mol^{-1} PTMG methyl methacrylate based graft-IPNs. An edge notch of 3 mm in length was cut into the samples, and the notch tip was sharpened using a razor blade.

An Instron 4465 universal testing machine was used for loading the specimen in tension and in displacement control mode (crosshead speed = 1mm/min). The load-deflection data was recorded up to crack initiation and during stable crack growth, if any. The crack initiation toughness or critical stress intensity factor, K_{IC}, was calculated using the load (F) recorded at crack initiation. For each graft-IPN category, at least three sets of experiments were performed at laboratory conditions. The mode-I stress intensity factor for a single edge notched (SEN) tensile strip using linear elastic fracture mechanics is given by Equation (2) [69],

$$K_{Ic} = \frac{F\sqrt{\pi a}}{Bw} f\left(\frac{a}{w}\right) \quad (2)$$

where,

$$f\left(\frac{a}{w}\right) = \left[1.12 - 0.23\left(\frac{a}{w}\right) + 10.6\left(\frac{a}{w}\right)^2 - 21.7\left(\frac{a}{w}\right)^3 + 30.4\left(\frac{a}{w}\right)^4\right]$$

and a is the edge crack length, w is the specimen width, B is the specimen thickness and F is the peak load.

Tensile Analysis

To characterize the tensile properties of graft-IPNs in terms of the elastic modulus, yield and ultimate stresses, quasi-static tension tests were performed. For quasi-static tension tests, the cured graft-IPN sheets were machined into dumbbell shaped specimen, which was inspired from ASTM D638 test method [70]. The size of the sheets that could be prepared precluded a complete adherence to ASTM standards.

An Instron 4465 universal testing machine was used for loading the specimen in tension and in displacement control mode (crosshead speed = 1 mm/min). An extensometer with 0.25" gauge length was used to record the strain. The load vs strain data was recorded up to 7 % strain for 650 g mol^{-1} PTMG methyl methacrylate based graft-IPNs and up to 20% strain for 1400 g mol^{-1} PTMG methyl methacrylate based graft-IPNs. Using the geometry of the specimen, stress was evaluated from load measurements to obtain stress vs strain data.

For each graft-IPN category, at least three sets of experiments were performed at laboratory conditions. The elastic modulus was evaluated from the slope of the stress-strain curve at less than 2% strain.

Stress relaxation measurements

Stress relaxation tests were carried out on samples on a TA Instruments Rheometrics Solids Analyzer, RSA III, by three-point bending. The tests were performed at temperatures of 25, 60 and 70 °C. Each sample analyzed was strained by 0.1% and the stress relaxation modulus, E(t), decay was recorded as a function of time (t). A 1 min delay was applied before the beginning of the experiment to allow the samples to equilibrate at test temperature.

RESULTS AND DISCUSSION

Analysis of FTIR measurements

In order to monitor the polymerization process of the polyurethane network infrared spectra were recorded. The analysis if based on the peak change of the functional group isocyanate (NCO) and acrylic double bond during the reaction time. The isocyanate absorption band is assigned at approximately 2300-2200 cm^{-1} in the mid infrared spectrum and its decay can be used to follow the conversion of the NCO group during the polymerization. For scaling the decrease of the NCO absorbance, the C-H stretch absorption (approx. 2960 cm^{-1}) was used as an internal standard as shown in Figure 11, since its concentration does not change during the reaction.

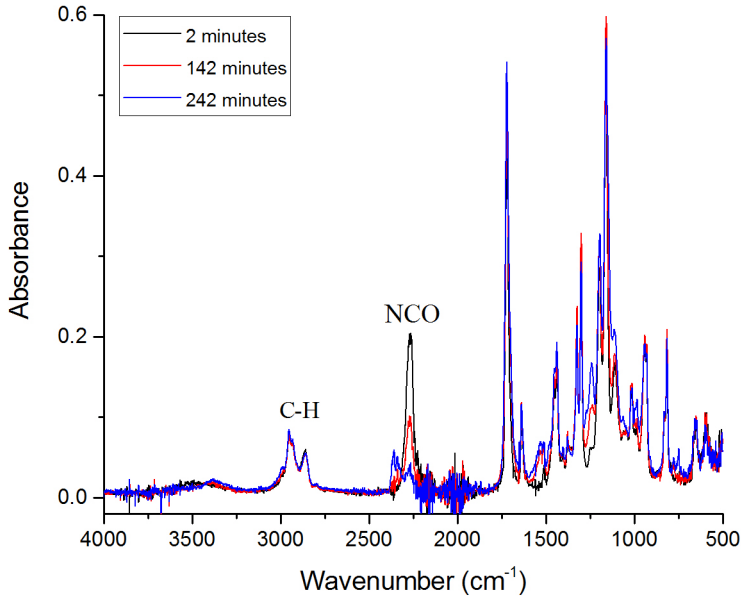

Figure 11. FTIR of graft-IPNs at different times during the curing process.

For the analysis it was assumed that there are no side reactions, and the isocyanate conversion was calculated as follows:

$$\text{Isocyanate conversion (p)} = 1 - \frac{(A_{NCO}/A_{CH_2})}{(A_{NCO}/A_{CH_2})_0} \quad \text{Equation (3) [71]}$$

Where A_{NCO} is the integrated absorbance for the isocyanate group, A_{CH2} is the integrated absorbance for the CH_2 group and $(A_{NCO}/A_{CH2})_0$ is the relative absorbance extrapolated for time zero. All experiments were carried out at temperatures and times use for the synthesis of graft-IPNs. Figure 12 shows the results from the FTIR experiments and the corresponding NCO conversion curves.

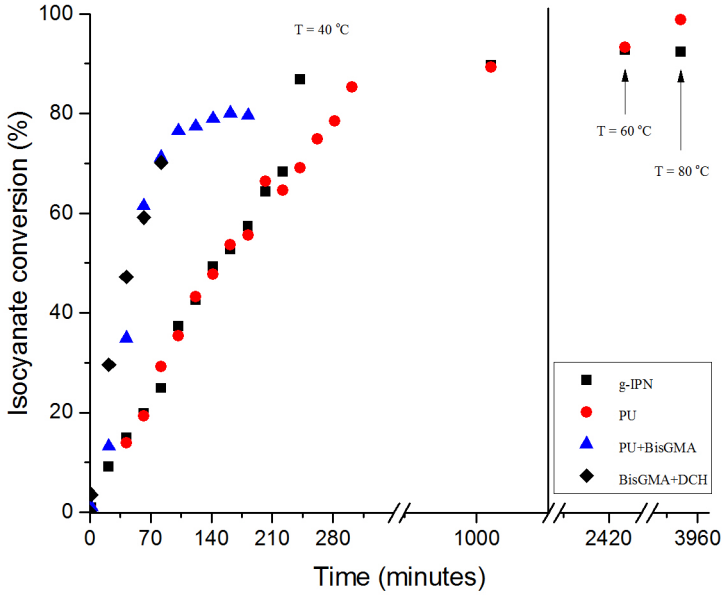

Figure 12. Isocyanate conversion plot.

The samples analyzed by infrared spectroscopy were: 70:30 copolymer:PU graft-IPN, pure PU, PU + BisGMA and DCH + BisGMA. All samples were synthesized using the 650 g mol^{-1} PTMG. From figure 12 it can be seen that the PU network and the graft-IPN reached very similar conversion values after 3900 minutes of reaction. One can also notice that the conversion value for the NCO on the graft-IPN sample was close to 93 %. For this sample in particular a NCO conversion above 82 % is an indication of the reaction of the secondary hydroxyl groups present in the BisGMA resin with free NCO groups in the PU network.

Since 18 % of the total NCO present in the sample is added with the solely purpose of generating grafts between networks, this means that 62 % of the total possible grafts were generated during the reaction time. Moreover, by analyzing these curves it seems that the presence of the methyl methacrylate monomer does not have a strong influence in the formation of the PU network in the graft-IPN system, since their conversion curves are practically overlapping. Figure 12 also shows how similar the PU + BisGMA and DCH + BisGMA conversion curves are.

One could speculate that the secondary hydroxyl groups from the BisGMA resin are reacting throughout the entire reaction time and not only when the primary hydroxyl groups coming from the PTMG and TRIOL are depleted. Regarding the follow up of the copolymer network formation, the conversion of the acrylic double bonds absorption band in the 1630-1650 cm^{-1} was monitored. Although since the data was gathered in the solid state rather than the liquid stated, the data collected was not sufficiently accurate to allow a proper determination of the final double bond conversion of the copolymer network present in the sample. The extent of reaction at the gel point was determined experimentally and theoretically for the samples

under analysis. The latter was obtained using Flory and Stockmayer statistical approach to gelation as describe elsewhere [72]. From Table 4 it can be seen that the extent of reaction determined experimentally are really close to the theoretical ones.

Table 4. Determination of extent of reaction at gel point.

Sample	Gel time (minutes)	Conversion at gel time (Experimental)	Conversion at gel time (Flory & Stockmayer)
graft-IPN	242	87 %	82 %
PU	222	69 %	79 %
PU + BisGMA	182	80 %	82 %
DCH +BisGMA	--	--	--

Thermo-mechanical characterization

The variables studied in the present work included the ratio of copolymer to PU, the molecular weight of poly (tetramethylene ether) glycol (PTMG) and the acrylic monomer employed to synthesize the copolymer phase. The ratio between the di- to tri-functionalized monomers (PTMG:TRIOL) for the PU phase was kept constant, since it is related to the crosslink density of the PU network. The ratio between the acrylic monomers to BisGMA resin was also kept constant. The number of possible crosslinks between networks is bounded by the reaction of secondary OH groups present in the BisGMA resin and the free isocyanate groups present in the PU network. If the acrylic monomer to BisGMA ratio were to be

changed, the moles of the latter resin would change, thus, altering the number of secondary OH group available for grafting.

All variables under study showed a major impact in the storage modulus of the systems. However, only the ratio of copolymer to PU and the acrylic monomer used had a significant effect on the T_g of the systems. Figure 13 and 14 show the thermo-mechanical properties (storage modulus, E′, and tan δ) of the graft-IPNs synthesized using the 650 g mol^{-1} PTMG as a function of temperature. In addition, Table 5 summarizes the results for all the different systems studied.

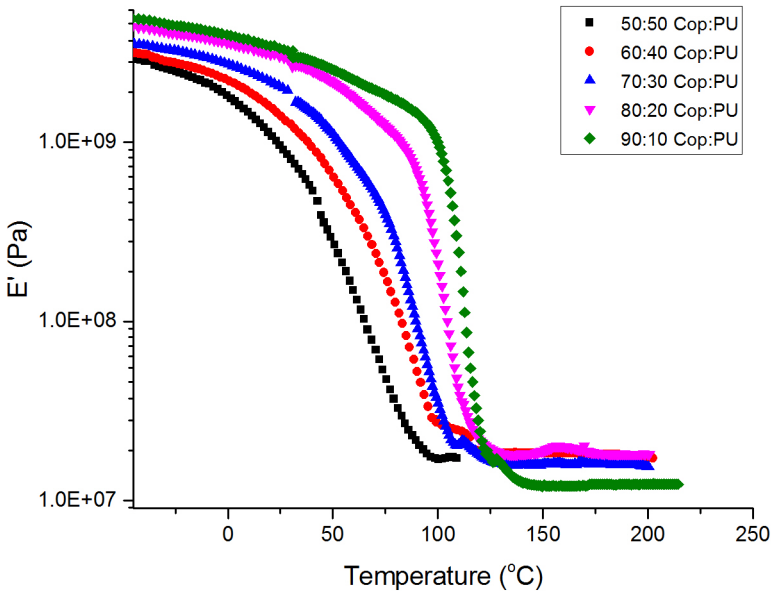

Figure 13. DMA results showing change in the storage modulus for graft-IPNs with various ratio of MMA based copolymer to 650 g mol^{-1} PTMG based polyurethane.

For all systems under study, it was observed that as the copolymer content increased, the samples exhibited higher values for the storage modulus, E′; a highly expected result since the copolymer phase provides the stiffness to the system. Samples consisting of 90 wt% copolymer showed a storage modulus of 3.35, 2.73 GPa at 25°C for the 650 and 1400 g mol^{-1} PTMG methyl methacrylate based graft-IPNs. While for the TEGDMA based graft-IPNs a value of 5.28 GPa at 25°C was obtained using the 650 g mol^{-1} PTMG. Samples containing less than 70 wt% of copolymer showed inferior values for the storage modulus, which can be attributed to the elastomeric contribution of the PU phase.

When comparing the systems with different molecular weight PTMGs, a substantial difference in the storage modulus was observed. As shown in Table 5, the storage modulus values for the system using the 1400 g mol^{-1} PTMG are inferior to those of the 650 g mol^{-1}. This reduction in the storage modulus may be explained by the higher mobility that a longer macrodiol provides to the PU network [62]. When analyzing the storage modulus of the TEGDMA-based samples (see Table 5), it can be seen that the substitution of a single double bond monomer (MMA) in the copolymer for a monomer with two double bonds (TEGDMA) had a major impact on the storage modulus. Samples containing this dimethacrylate monomer had a tendency to present higher storage modulus than those synthesized using MMA.

As described by Heatley and coworkers [73], BisGMA-TEGDMA copolymers are characterized by presenting high degrees of crosslinking, due to presence of two double bonds in their chemical structures, which generated more crosslink points within the copolymer network, resulting in an increase in the crosslink density of the network. This increase in the crosslink density diminished to a certain extent the mobility of the network

chains, increasing the stiffness of the system, thus, increasing the storage modulus of the samples. To corroborate this statement, the M_C of the MMA and TEGDMA graft-IPNs were experimentally estimated by measuring the equilibrium storage modulus in the rubbery state, using the Equation (1) from the theory of rubber elasticity. The samples analyzed were the 70 % copolymer content using the 650 g mol^{-1} PTMG. The results showed M_C values of 910 and 72 g mol^{-1} for the MMA and TEGDMA samples respectively. As expected the dimethacrylate-based sample showed the lowest value for M_C, which as stated earlier, provides an explanation for the higher values of storage modulus obtained for all TEGDMA-based samples over its MMA-based counterparts. Figure 14, shows the plot of tan δ as a function of temperature for the MMA based graft-IPNs synthesized using the 650 g mol^{-1} PTMG.

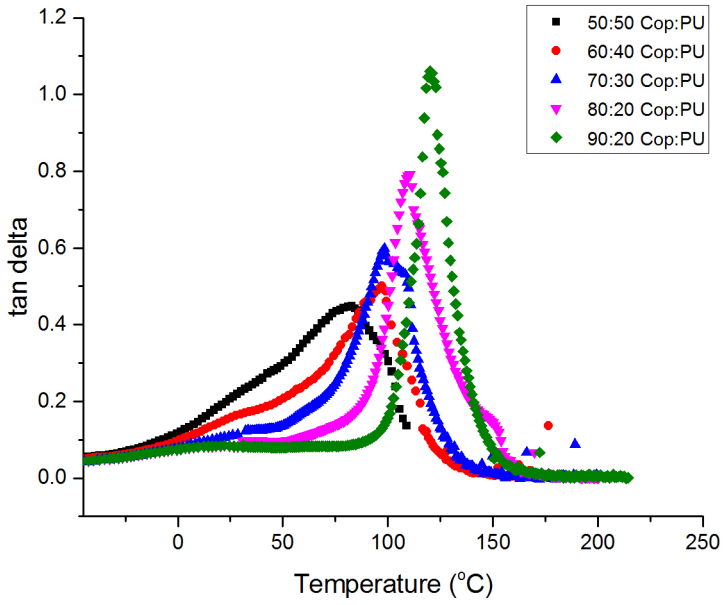

Figure 14. DMA results showing change in tan δ for graft-IPNs with various ratio of MMA based copolymer to 650 g mol^{-1} PTMG based polyurethane.

In this graph, a maximum peak of the loss factor showed the characteristic relaxation associated with the glass transition temperature of the different systems under study. It was observed that as the weight percentage of copolymer increased in the samples, the maximum peak of the loss factor gained prominence and moved to higher temperatures.

The narrow peak of the loss factor in the sample with 80 and 90 % copolymer content suggested a high degree of miscibility. For the rest of the samples a broad transition with a shoulder related to the glass transition of the PU phase was observed in the curves, which it is characteristic of a partially miscible system. A similar peak in the loss factor for the 90 % copolymer content was also observed for the composition using the 1400 g mol^{-1} PTMG, as well as broader transitions for samples containing < 90 weight percentages of copolymer. This suggests that several different relaxation mechanisms are present in the produced network, and they may be related to the nano-heterogeneity of the system [62, 53].

In the case of the TEGDMA-based graft-IPNs, all samples presented broad transitions, also suggesting a high level of heterogeneity in the system. However, in the case of dimethacrylates, the heterogeneity formed, as explained by Podgórsky. M [74], results from highly crosslinked structures in which a broad distribution of micro-domains can be found. This kind of polymer networks have shown both loosely connectivity and highly crosslinked regions, as well as regions were unreacted monomer is present. This lack of homogeneity in the network structure has as a result the manifestation of a broad distribution of relaxation times due to the matrix mobility.

Table 5. Storage modulus, E′, glass transition temperature, T_g, storage modulus at the rubbery plateau, E_R, and M_C for the different graft-IPNs synthesized.

Sample	Copolymer content (wt%)	E′ (Pa) at 25°C	T_g (°C)	E_R (Pa)	M_C (g mol^{-1})
Graft-IPN with 650 g mol^{-1} PTMG	90	3.35 x 10^9	120	1.20 x 10^7	890
	80	3.02 x 10^9	110	1.80 x 10^7	637
	70	2.07 x 10^9	98	1.57 x 10^7	910
	60	1.40 x 10^9	97	1.84 x 10^7	655
	50	0.96 x 10^9	83	--	--
Graft-IPN with 1400 g mol^{-1} PTMG	90	2.73 x 10^9	120	1.04 x 10^7	1360
	80	2.36 x 10^9	107	1.36 x 10^7	907
	70	1.39 x 10^9	97	9.77 x 10^6	1265
	60	0.95 x 10^9	83	1.18 x 10^7	1030
	50	0.41 x 10^9	72	--	--
Graft-IPN with 650 g mol^{-1} PTMG Tri-EDMA	90	5.28 x 10^9	141	--	--
	80	4.41 x 10^9	121	--	--
	70	1.08 x 10^9	118	1.73 x 10^8	72
	60	0.62 x 10^9	116	--	--

Network Morphology

The network morphology of the graft-IPN was studied to corroborate the improvement achieved in the interpenetration of the two polymer networks as a result of the chemical crosslink between networks. Figure 15 shows TEM photos of sections cut from stained methyl methacrylate copolymer based graft-IPN samples containing 70% copolymer content with different molecular weight PTMGs at different stages of the curing process. Here, the dark zones correspond to PU regions, since the PU phase is the one that absorbed the dye, while the clear zones correspond to the copolymer phase.

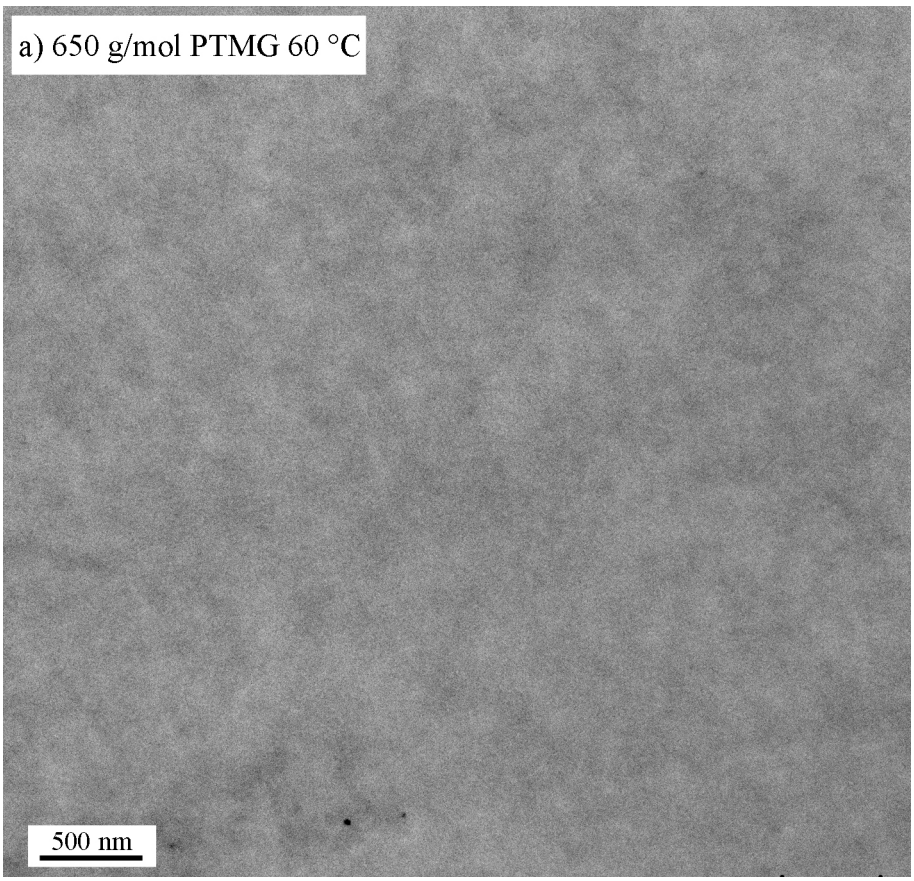

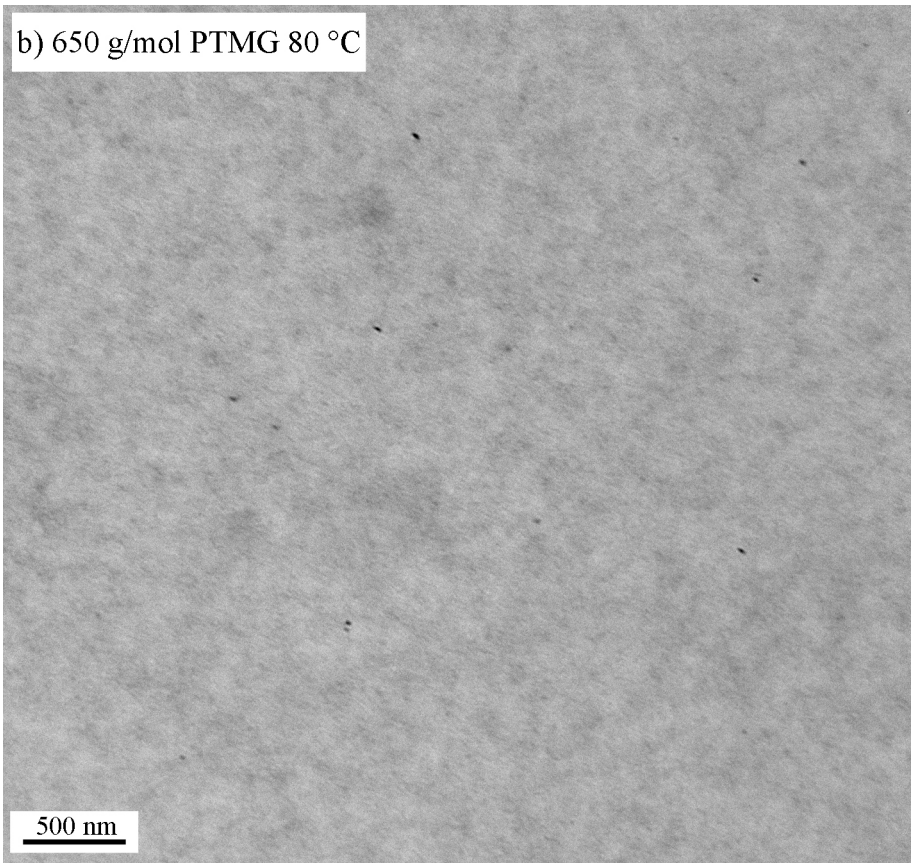
b) 650 g/mol PTMG 80 °C
500 nm

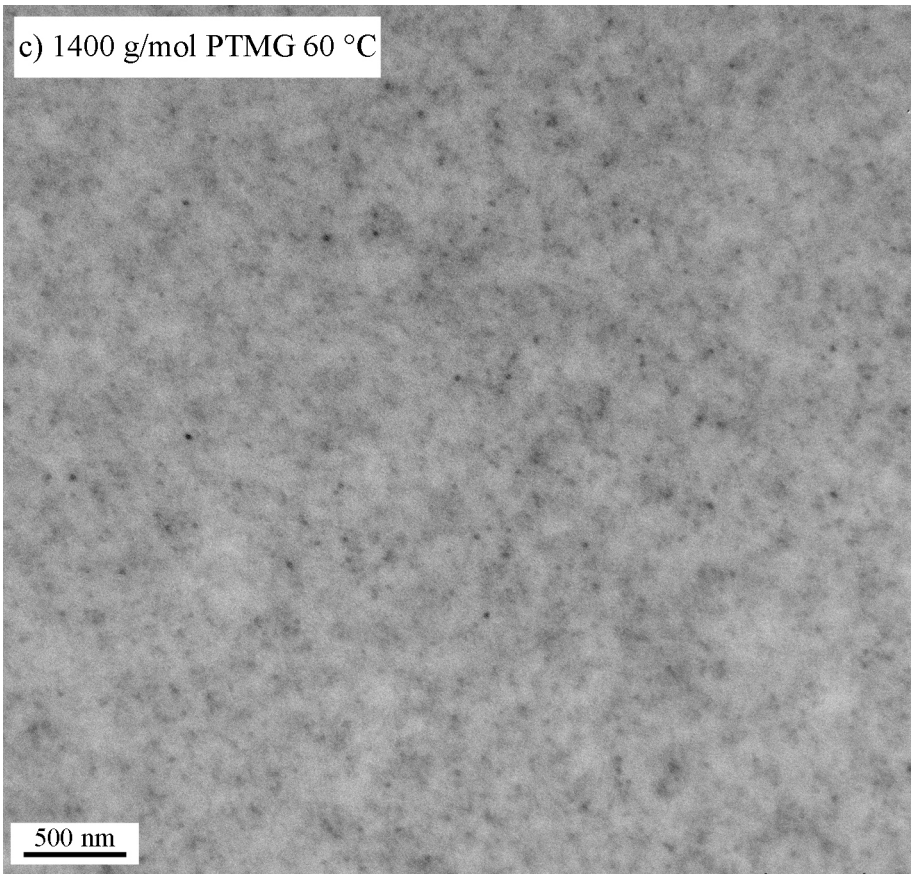
c) 1400 g/mol PTMG 60 °C
500 nm

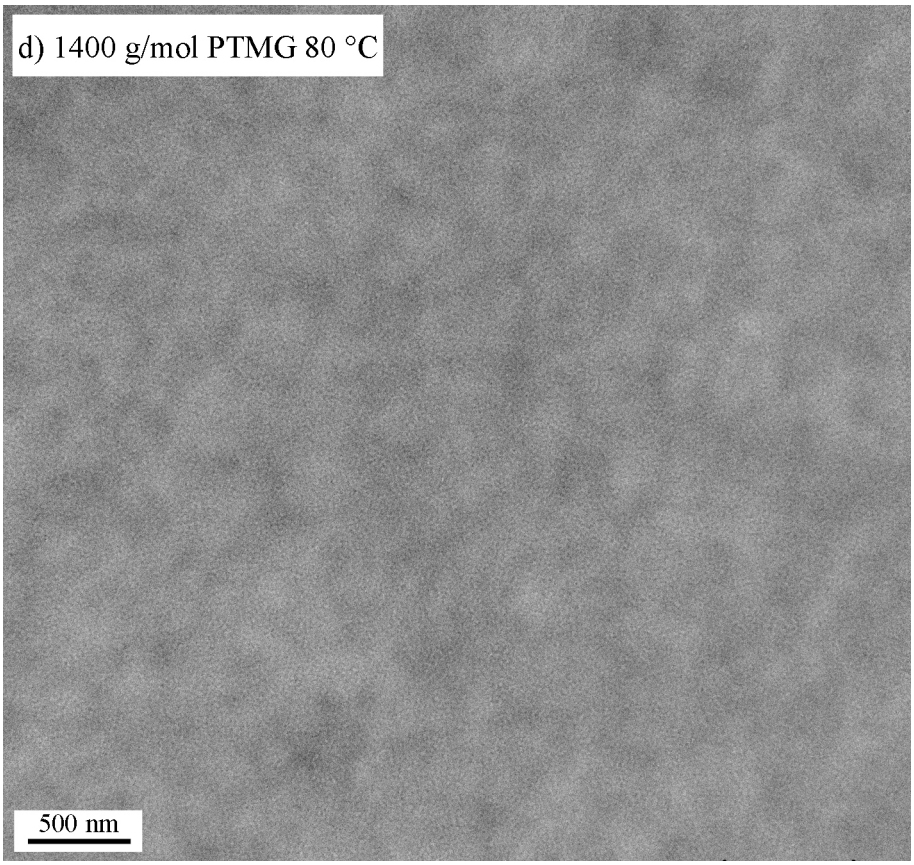

Figure 15. TEM photos of graft-IPNs with 70 wt% MMA based copolymer using the 650 g mol^{-1} PTMG at (a) 60 °C, (b) 80 °C and 1400 g mol^{-1} (c) 60 °C and (d) 80 °C.

In general, the morphology presented by different IPNs is rather complex, since different competing processes may occur simultaneously during polymerization. In sequential polymerization; as is the case in this work, the formation of the first network has a major impact on the formation of the second, limiting the range of compositions and the material's final properties obtained by following this synthetic route.

As shown in Figure 15c, it appears to be a slight formation of PU domains for the 1400 g mol^{-1} PTMG graft-IPNs at 60 °C. As the curing process of the samples was finalized after 24 h at 80 °C, the PU domains seemed to disappear (see Figure 15d). This observation may be

explained by further formation of crosslink points between the two networks by means of the reaction between the hydroxyl groups present in the BisGMA resin with the isocyanate groups present in the PU phase.

These TEM pictures are a corroboration of the decrease in size of these domains by the formation of the aforementioned crosslinking points, which improved the system's miscibility, thus minimizing the phase separation between networks [62]. Furthermore, when comparing the two graft-IPNs with different molecular weight PTMGs, it can be seen from the TEM pictures that both systems presented a fine dispersion of both networks through the entire sample. This is attributed to the successful interpenetration of the two different networks at the molecular level [53].

Degree of transparency

Transparency of the MMA based copolymer using the 650 and 1400 g mol^{-1} PTMG samples synthesized was analyzed. The system presented a relative high degree of transparency, showing values of transmittance between 65 and 90%, as shown in Figure 16a.

a)

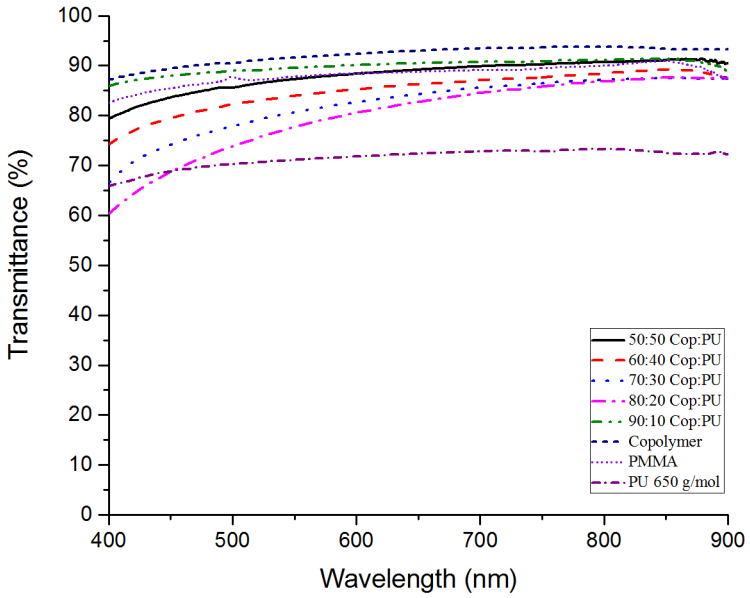

b)

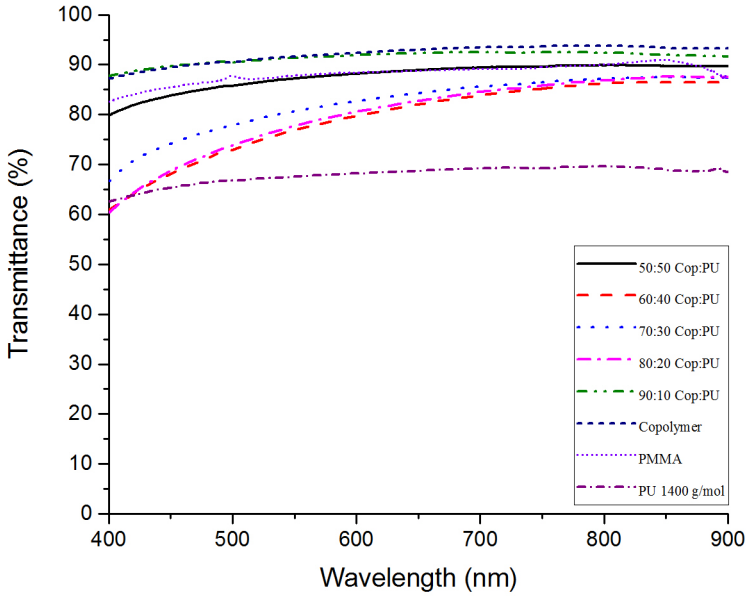

Figure 16. UV-vis spectrum of MMA based copolymer and a) 650 g mol^{-1} PTMG based polyurethane and b) 1400 g mol^{-1} PTMG based polyurethane graft-IPN.

The same degree of transparency was also observed for the 1400 g mol^{-1} PTMG based system, as seen in Figure 16b.

These results are also confirmation of the high degree of interpenetration achieved on both systems regardless of the molecular weight of the PTMG. There is no visible evidence of macroscopic phase separation in the samples studied, supporting the results shown in the plot of tan δ as a function of temperature.

Stiffness and fracture toughness

The stress versus strain plots obtained from the tension tests in case of 650 and 1400 g mol^{-1} PTMG are shown in Figure 17a and 17b respectively. These results were obtained from Dr. Tippur's research group in the Department of Mechanical Engineering at Auburn University, Alabama. It can be seen that the modulus and the peak stress drops progressively with increase in PU resulting in no observed failure within the window of imposed strains.

a)

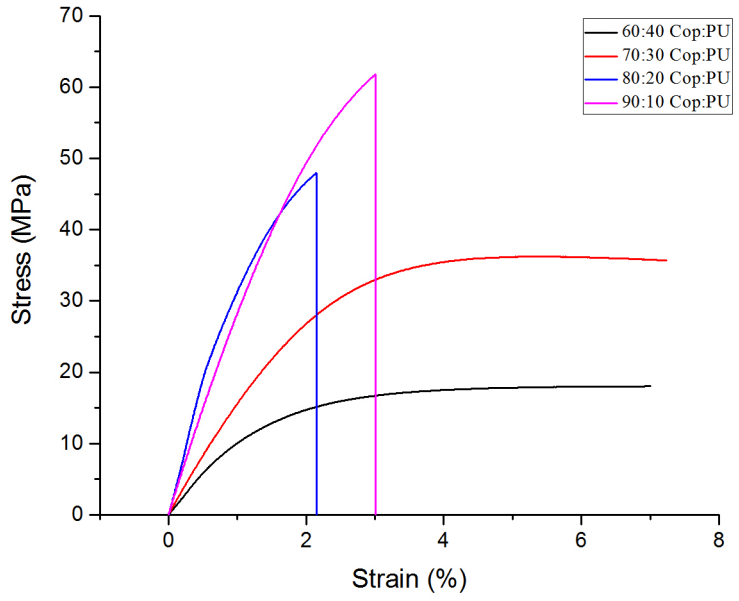

b)

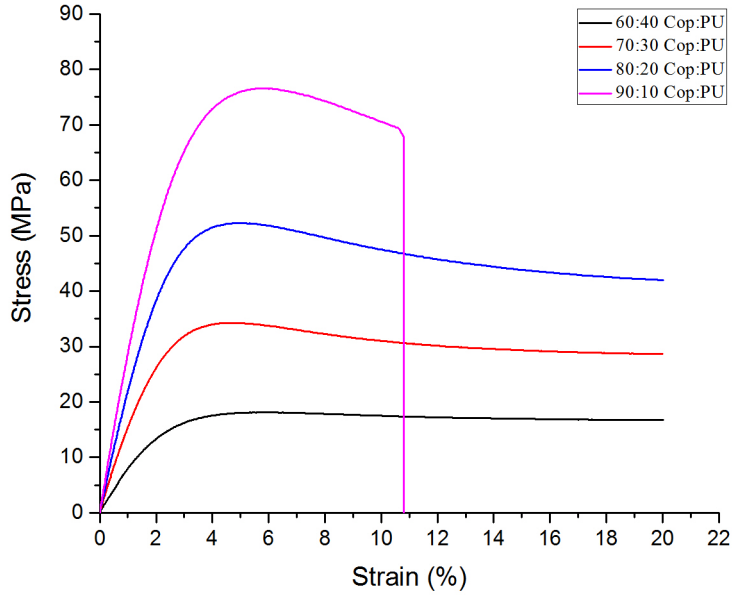

Figure 17. Stress vs Strain plots for MMA based copolymer samples using (a) 650 g mol^{-1} PTMG and (b) 1400 g mol^{-1} PTMG based polyurethane during tension test.

Table 6 shows results obtained for the quasi-static crack initiation toughness, K_{IC} for the graft-IPNs studied. When both systems are compared, it can be seen that the graft-IPNs synthesized with the 1400 g mol^{-1} PTMG have a slightly higher value for the quasi-static crack initiation toughness than those synthesized using the 650 g mol^{-1} PTMG. Furthermore, it can be observed that both systems displayed the highest value of fracture toughness in samples with a 70% of copolymer content, suggesting that there is an optimum copolymer to PU ratio.

Table 6. Results obtained for the fracture toughness tests performed on different graft-IPNs synthesized.

Sample	Copolymer content (wt%)	K_{Ic} (MPa $m^{1/2}$)	E (GPa)	Ultimate stress (MPa)	Failure strain (%)
Graft-IPN with 650 g/mol PTMG	90	1.17±0.03	3.3±0.05	61.79	3.05
	80	1.16±0.14	3.6±0.03	47.97	2.155
	70	2.70±0.09	2.2±0.02	35.78	>7
	60	1.84±0.06	1.3±0.04	18.06	>7
Graft-IPN with 1400 g/mol PTMG	90	1.49±0.05	3.4±0.05	76.50	10.80
	80	2.35±0.08	2.65±0.08	52.29	>20
	70	2.95±0.12	2.5±0.11	34.27	>20
	60	1.73±0.04	1.2±0.08	18.11	>20
Graft-IPN with 650 g mol^{-1} PTMG TEGDMA	70	0.77±0.02	-	-	-

Determination of average molecular weight between crosslinks (M_C) and its relation with fracture toughness.

The average molecular weight between crosslinks for the MMA based graft-IPNs was experimentally obtained by measuring the storage modulus in the rubbery plateau, E_R, at 50 °C above the glass transition temperature according to the Equation (1) from the theory of rubber elasticity.

In previous studies done by Karger-Kocsis and coworkers [75], Liang and coworkers [76], Liu and coworkers [77], a linear correlation between the fracture toughness and M_C was found. It was seen that as M_C increased in the system the higher the K_{IC} value became. Sherman and coworkers [78] attribute this to an increase in the free volume of the materials, which allows more space resulting in an increase of chain motions capable to accommodate the applied load. Nevertheless, a linear correlation was not found for the system under study, the results showed that the K_{IC} values did not increase as M_C increased, which seems to suggest that a different mechanism is responsible for the increase in the fracture toughness displayed by graft-IPNs. This tendency holds true for both 650 and 1400 g mol^{-1} PTMG based graft-IPNs, as seen in Figure 18a and Figure 18b.

a)

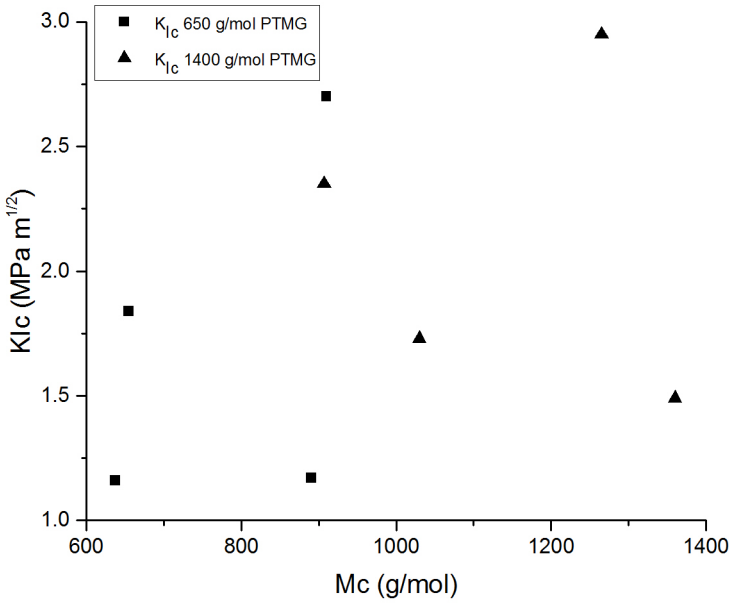

b)

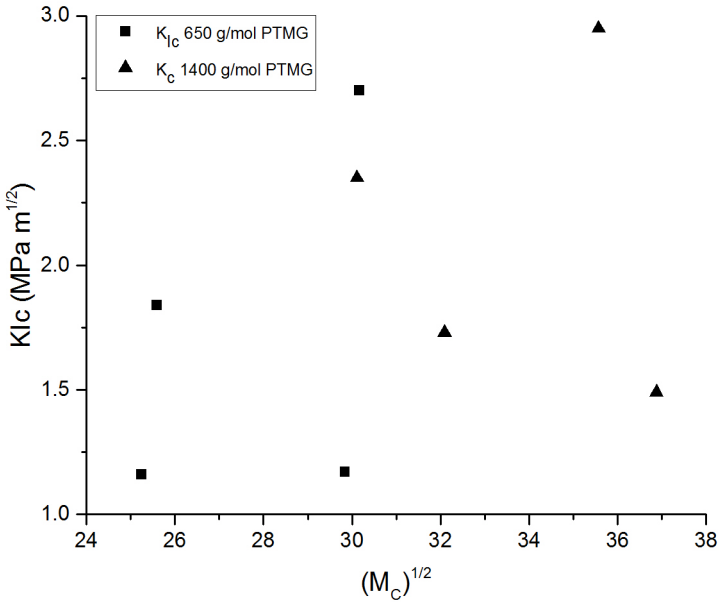

Figure 18. Plot of (a) K_{1c} vs M_C plot and (b) K_{1c} vs $M_C^{1/2}$.

Surface Morphology

In order to study the fracture mechanics of the graft-IPN systems, SEM images were taken from samples used for fracture testing. Figure 19 shows the fractured surfaces of graft-IPNs samples with different copolymer to polyurethane ratios for the graft-IPNs synthesized using the 1400 g mol^{-1} PTMG.

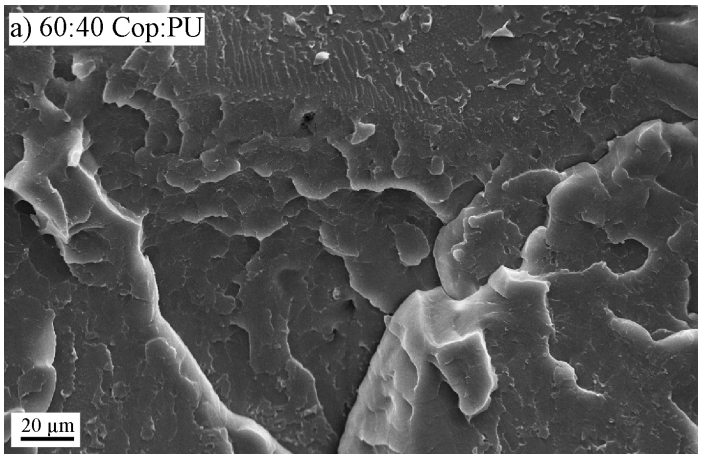

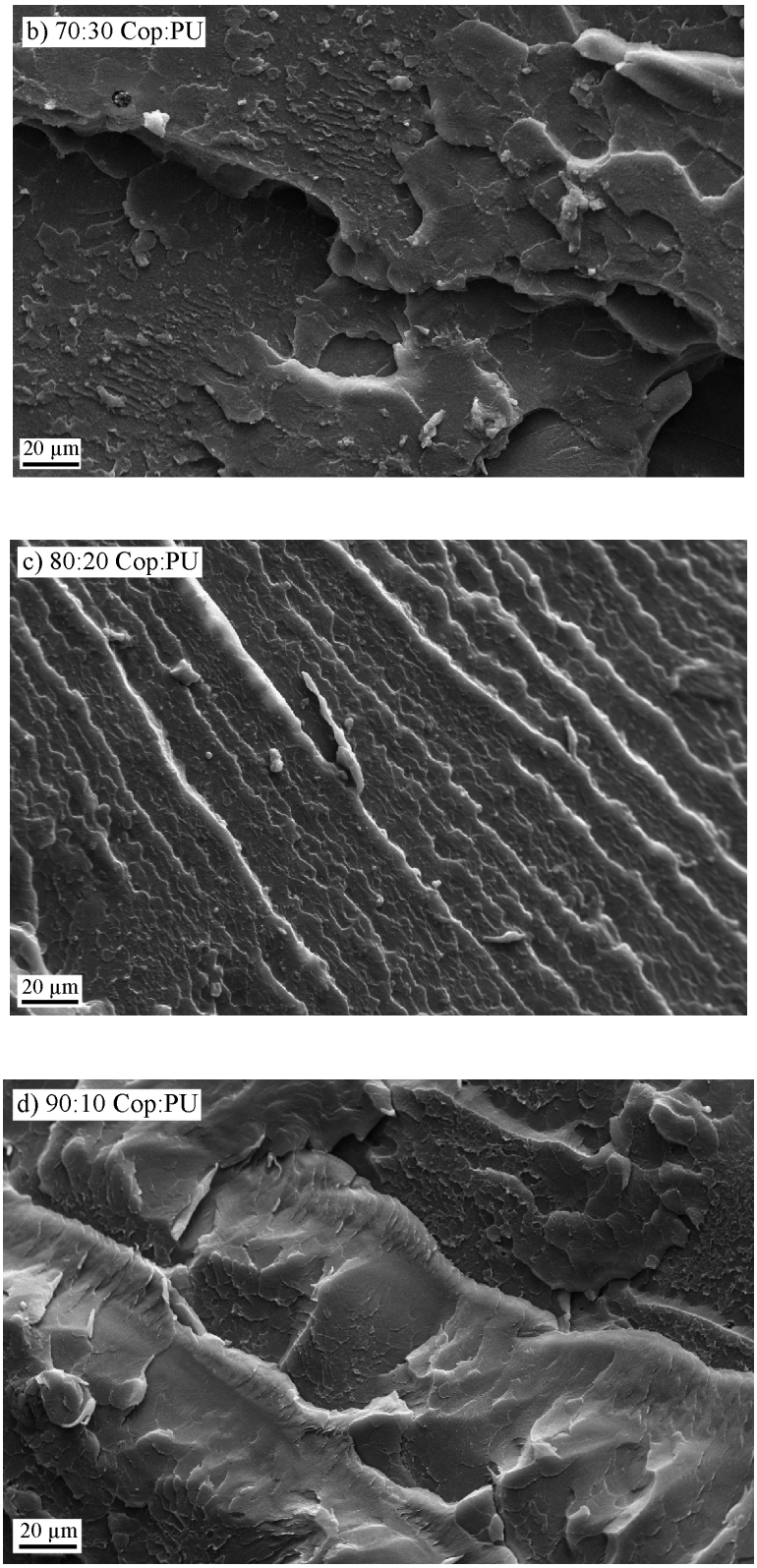

Figure 19. SEM photos of (a) 60 wt% copolymer, (b) 70 wt% copolymer, (c) 80 wt% copolymer and (d) 90 wt% copolymer MMA based graft-IPNs samples using the 1400 $gmol^{-1}$ PTMG.

From Figure 19, it can be seen that regardless of PU content present in the samples, this factor does not have a significant effect on the surface area created were the fracture propagated through the material. When compared to previous work done by Bird and coworkers [53], the authors were able to observe how an increase in the PU content in the system resulted in an increase on the surface area were the fracture propagated through the material. They also observed how the samples with a higher PU content had better fracture toughness values, which led them to correlate the surface area generated during fracture testing with the fracture toughness properties of the material.

However, this correlation between an increase of surface area and fracture toughness was not observed on the graft-IPN systems. Although it was possible to see how samples with a copolymer content equal or superior to 80 % show brittle fractures while samples under 80 % copolymer content show did not show a brittle fracture. These results suggest that a different fracture mechanism is responsible for the improvement in the fracture toughness values presented by the graft-IPN.

Stress relaxations of graft-IPNs

The data of three-point bending stress relaxation analysis of graft-IPNs at different temperatures are shown in Figure 20. In this figure, the relaxation modulus, E(t), measured at three different temperatures is normalized with respect to the initial relaxation modulus in order to obtain $E_n(t)$, and then plotted as a function of time.

a)

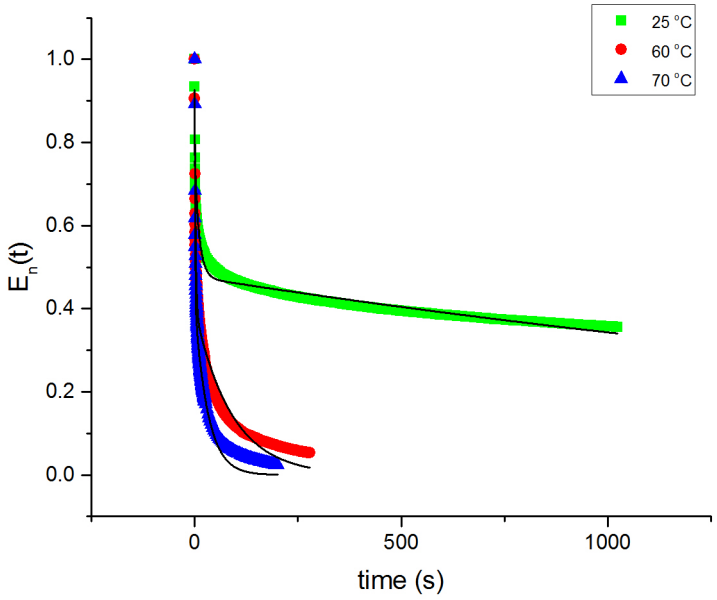
25 °C
60 °C
70 °C
1.0
0.8
0.6
0.4
0.2
0.0
E_n(t)
0
500
1000
time (s)

b)

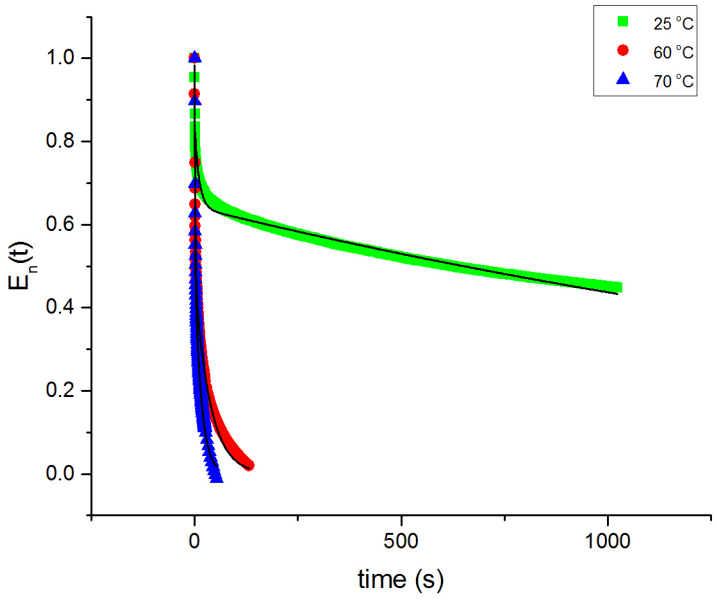
25 °C
60 °C
70 °C
1.0
0.8
0.6
0.4
0.2
0.0
E_n(t)
0
500
1000
time (s)

c)

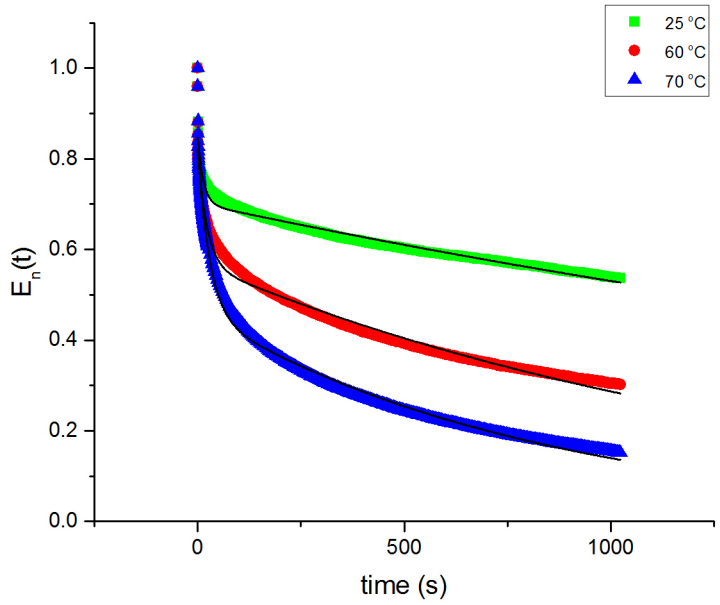
25 °C
60 °C
70 °C
1.0
0.8
0.6
0.4
0.2
0.0
E_n(t)
0
500
1000
time (s)

d)

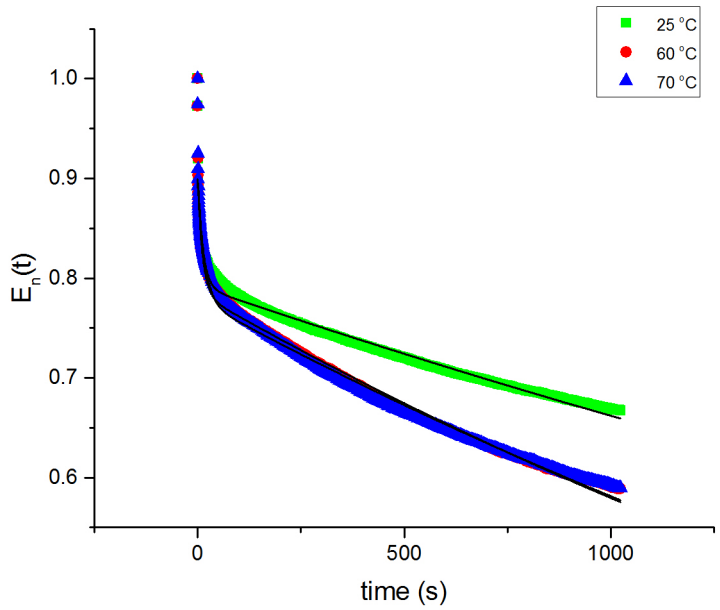
25 °C
60 °C
70 °C
1.0
0.9
0.8
0.7
0.6
E_n(t)
0
500
1000
time (s)

e)

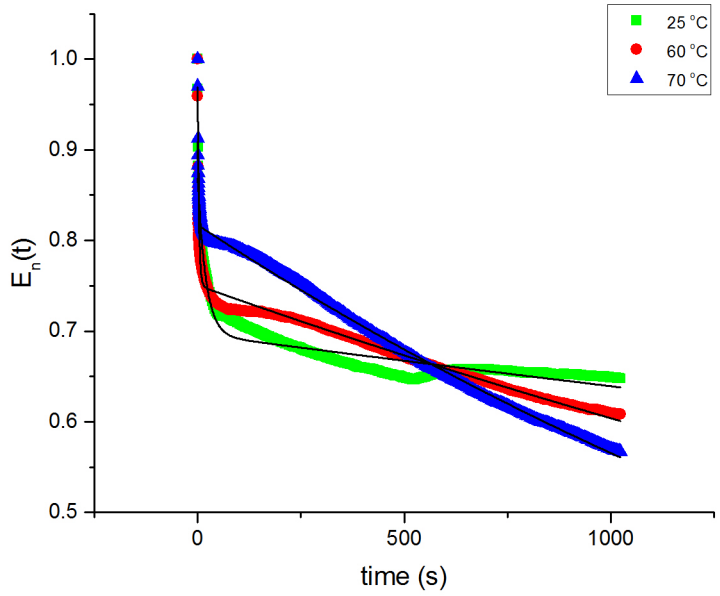

Figure 20. Normalized stress relaxation modulus for graft-IPNs with different copolymer content, a) 60%; b) 70%; c) 80%; d) 90%, and e) 100% at three different test temperatures.

It can be observed from Figure 20 that relaxation modulus decreases with an increase in the temperature and time. Moreover, in general all relaxation curves showed a negative slope even after the test was completed. These results clearly indicate that the samples were still relaxing after the test's time frame and they did not reach the equilibrium relaxation modulus. From Table 7, it can be seen that in most of the compositions analyzed the E(t) decreased as the test temperature increased, this kind of behavior indicates a predominance of the viscous component at higher temperatures due to an increase of free volume of network, resulting in chain movements [82].

Table 7. Initial stress relaxation modulus of graft-IPNs at different temperatures and copolymer weight percentage.

	60 wt%	70 wt%	80 wt%	90 wt%	100 wt%
25 °C	1.08 x 10^9 Pa	1.82 x 10^9 Pa	3.22 x 10^9 Pa	2.44 x 10^9 Pa	2.28 x 10^9 Pa
60 °C	3.26 x 10^8 Pa	7.53 x 10^8 Pa	1.46 x 10^9 Pa	1.63 x 10^9 Pa	1.36 x 10^9 Pa
70 °C	2.50 x 10^8 Pa	4.76 x 10^8 Pa	1.41 x 10^9 Pa	2.02 x 10^9 Pa	1.48 x 10^9 Pa

Modeling of Stress Relaxation Behavior of graft-IPNs

The stress-relaxation features of polymers are generally described by the stress relaxation time, τ, and the stress relaxation modulus, E(t). Barua and co-workers [83] described the relaxation time, τ, as a characteristic measure of time dependent stress decay, $\sigma(t)$, from a deformed state, σ_0, under a constant initial strain, ε_0. A general description of the relationship between the stress decay, $\sigma(t)$, the stress relaxation modulus, E(t), and the initial strain, ε_0 is given by Equation 4,

$$E(t) = \frac{\sigma(t)}{\varepsilon_0} \quad (4)$$

In this chapter, two different models were considered for modeling the stress relaxation behavior of graft-IPNs. The two models employed for this purpose were the biexponential Maxwell model, which yields two characteristic relaxation times (one fast, τ_f, and one slow, τ_s) [84], as given by

$$E_n(t) = \phi_f \exp(-t/\tau_f) + \phi_s \exp(-t/\tau_s) \quad (5)$$

where ϕ_f and ϕ_s are adjustable weighting factors that sum to nearly unity. The second model employed on this study was the Kohlrausch-Williams-Watts (KWW), commonly known as stretched exponential [85], which is given by

$$E_n(t) = exp[-(t/\tau)^b] \quad (6)$$

where b, is referred to as the stretching exponent, and takes values between zero and one. Table 8, summarizes all the experimental data obtained from the application of the two models to the stress relaxation curves of the graft-IPNs under study.

Table 8. Summary of the Stretched exponential and biexponential Maxwell stress relaxation times for graft-IPNs with different copolymer wt%.

Sample	Kohlrausch-Williams-Watts (KWW)			biexponential Maxwell					
	τ (s)			τ_f			τ_s (s)		
	25 °C	60 °C	70 °C	25 °C	60 °C	70 °C	25 °C	60 °C	70 °C
60	790	11.25	5.50	11.1	2.4	1.1	3043	89.3	31.7
70	4777	9.0	-0.1	11.1	1.3	0.6	2600	36.8	15.9
80	21503	618	0.34	13.8	21.8	29.1	3578	1460	837
90	303940	23792	20506	12.7	12.0	16.3	5578	3297	3428
100	331705	368730	22772	19.7	3.5	1.5	11666	4603	2717

The application of the KWW model to the stress relaxation curves as shown in Figure 21, results in an unsatisfactory fit for all systems under study. However, the employment of the biexponential Maxwell quiet accurately describes the stress relaxation behavior of graft-IPNs. In order to compare the fit accuracy between models, a fit comparison was performed using the Akaike's information criterion test (AIC), a widely used test for model selection [83]. The evaluation of each model fit was carried out using the Origin graphing and analysis software on a personal computer. According to the AIC test, the biexponential Maxwell model is 7.38 e^{64} times more likely to be correct than the Stretch exponential model.

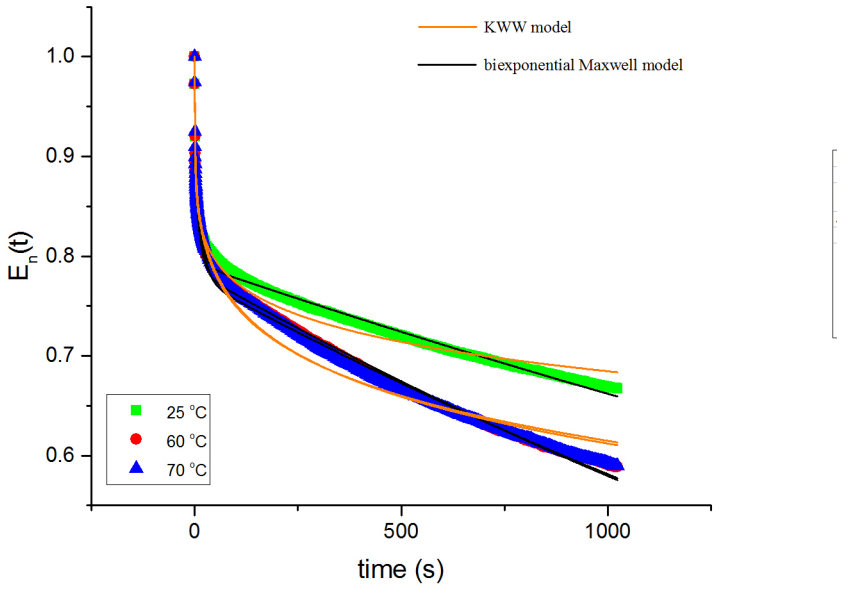

Figure 21. Fit comparison between the Stretch exponential model and the biexponentail Maxwell model for graft-IPN sample with a copolymer to PU ratio of 90:10.

The temperature dependence of τ_s on the reciprocal of temperature is shown in Figure 22. One can see that the long time component of the stress relaxation generally displays a typical Arrhenius behavior [86], which is described by

$$\tau_s = \tau_0 exp(Q_n/RT) \quad (7).$$

where τ_0 is a constant, Q_n is the activation energy, R is the gas constant and T denotes the absolute temperature. From Figure 22, it can be seen that there is a marked difference on the activation energy for systems with copolymer a content above 80% and the systems below 80%. One could speculate that the graft-IPN system undergoes a change in the stress relaxation mechanism when the copolymer content reaches 80%. Furthermore, as seen in the fracture test section, there is a clear change from a ductile behavior for samples under 80% copolymer content to a brittle behavior for samples above 70% copolymer content.

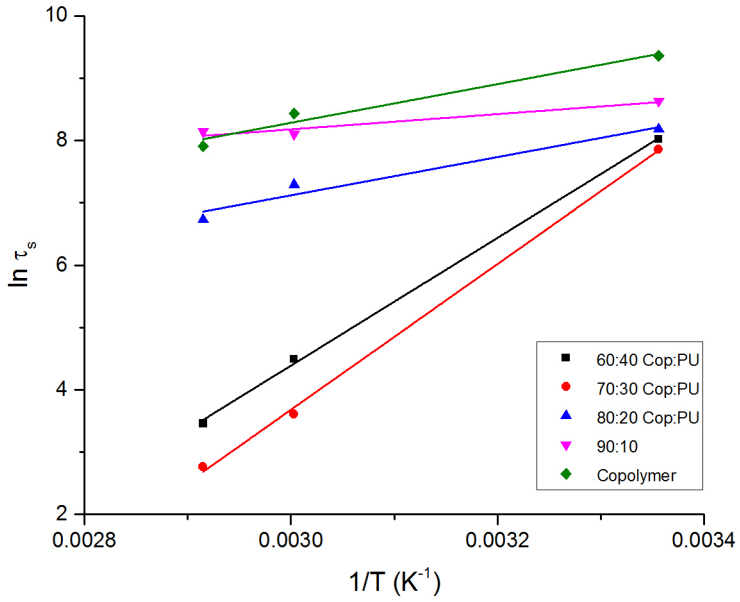

Figure 22. Temperature dependence of τ_s for gaft-IPNs with different copolymer content.

However, evaluation of Q_n from the values of τ_s shown in Figure 22 provides the data displayed in Figure 23.

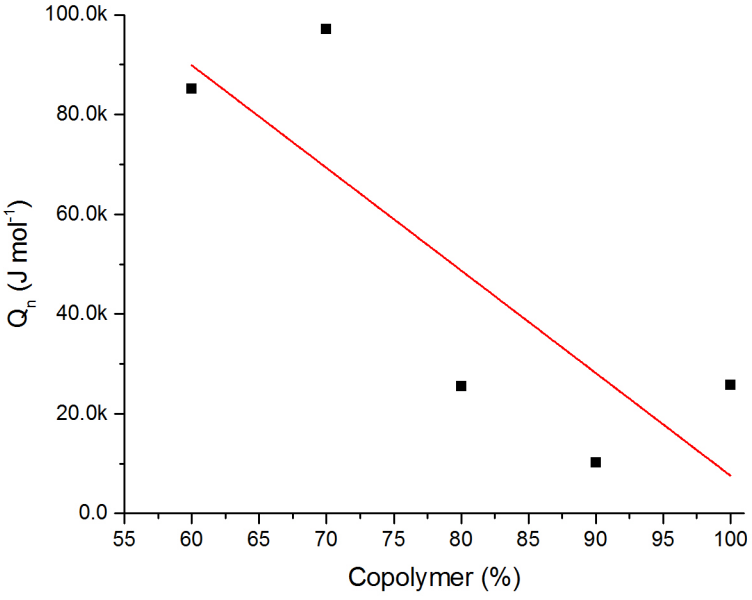

Figure 23. Relaxation activation energy, Q_n, as a function of copolymer content.

From Figure 23, it can be seen that in general terms, the graft-IPNs exhibited an Arrhenius-type behavior, which means that it seems to be direct composition-dependent effect in the segmental mobility of the graft-IPN system.

CONCLUSIONS

In this study, a series of graft interpenetrated polymer networks consisting of a polyurethane and a copolymer network were synthesized. Where, the influence of the copolymer to PU ratio, molecular weight of the PTMG and copolymer's chemical composition on the thermo-mechanical and fracture toughness properties, as well as both network and surface morphology were systematically studied.

As expected, the findings suggest that the toughenability of the graft-IPNs synthesized was highly dependent on all three aforementioned variables. It was found that samples comprise of 70 wt% MMA based copolymer and 1400 g mol^{-1} PTMG based polyurethane presented the best combination of high E′, T_g and fracture toughness of all systems under study. The network morphology studies showed that there is no clear domains in any of the samples analyzed, what suggests that phase separation was successfully minimize by the generation of crosslink points between the copolymer and PU networks by means of the BisGMA resin.

The surface morphology analysis suggests that a different fracture mechanism is accountable for the improvement in the fracture toughness presented by the graft-IPN systems, since there is no clear correlation between an increase on the fracture toughness and an increase in surface area were the fracture propagated in the samples. Additional work is still needed for understanding the fracture mechanism accountable for the high crack initiation toughness showed by graft-IPNs.

The stress relaxation behavior of different graft-IPNs was studied by means of three-point bending at three different temperatures. The stress relaxation analyses were carried out at a set strain of 0.1%. It was observed that the stress relaxation modulus decreased with time for most graft-IPN formulations. Moreover, the initial stress relaxation modulus was also found to decrease with an increase in the temperature. This effect is due to the predominance displayed by the viscous component at higher temperatures. The stress relaxation results were analyzed using the stretched exponential model and the biexponential Maxwell model. It was found that the biexponential model was far more accurate for the prediction of the stress relaxation behavior of the graft-IPNs systems.

CHAPTER III.

Vinyl ester-based graft-Interpenetrating Polymer Networks

INTRODUCTION

Vinyl ester resins,VE, are commonly synthesized by reacting acrylic acids with a bisphenol A-based epoxy resin, see Figure 22. Typically, bisphenol-A based dimethacrylate resins are characterized for their high viscosity. For this reason, vinyl ester resins are crosslinked using a low viscosity reactive monomer or diluent such as styrene [85].

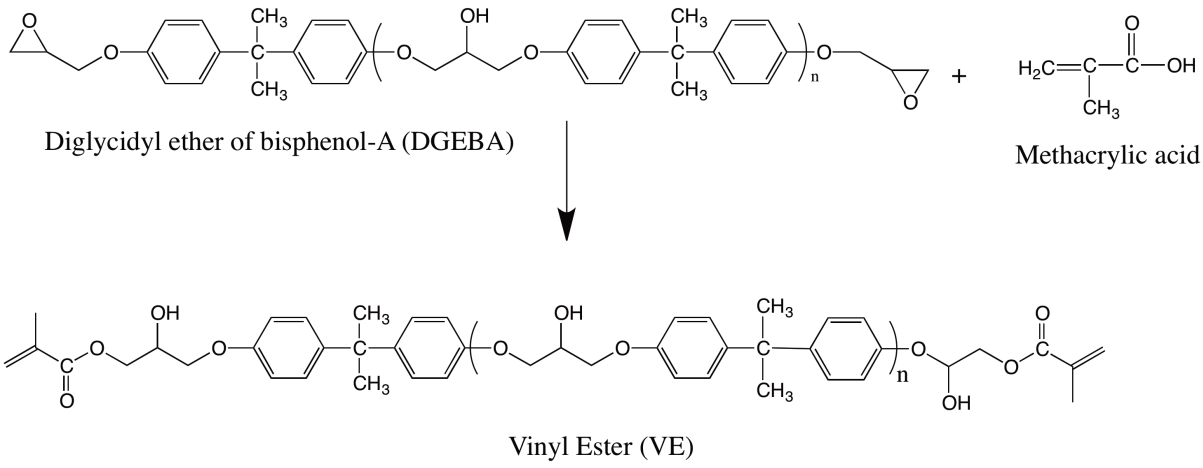

Figure 24. The methacrylation of DGEBA to form vinyl ester monomer, modified from reference [86].

Vinyl ester resins were developed in an attempt to combine the mechanical and thermal properties of epoxy resins with the fast curing process presented by unsaturated polyester

resins. This combination of properties makes them particularly interesting for applications in high-performance composites [87]. Moreover, vinyl ester resins are frequently used to make polymer matrix composites in both military and civilian applications due to their high modulus, low weight and low cost. When compared to unsaturated polyester systems, vinyl ester resins have superior properties as well as lower manufacturing costs and are easier to process than epoxy based systems [88].

However, a major disadvantage showed by vinyl ester resins is their brittle nature, which is translated in low fracture toughness. For this reason, many scientists and engineers have devoted their efforts to improve vinyl ester resins fracture toughness. Many different approaches have been taken in order to improve the toughness of vinyl ester resins including (a) modification of network structure by means of modifying VE's molecular weight and styrene content, (b) use of reactive and non-reactive rubber modifiers designed for phase separation upon cure, and (c) use of nanostructurated thermoplastics fiber mats for interlaminar toughening [89].

Nonetheless, all of these techniques present some limitations. For instance, little toughness improvement is achieved by modifying the network's structure. Rubber-toughened VE resins usually achieve better fracture resistance, however, the thermal resistance as well as the modulus of the original resin are severely compromised. In the case of using nanostructurated thermoplastic fiber mats, this generally results in complex and difficult processing problems [90].

Chen and co-workers [91] took a different approach in order to improve the vinyl ester toughness by incorporating a rubbery polymeric material into the system. In their work, they studied the synthesis as well as the thermal properties and morphology of simultaneous full-interpenetrating polymer networks, full-IPNs, based on blocked polyurethane, PU, and vinyl ester, VE, resin. However, the generation of chemical crosslinks between the networks by means of the hydroxyl groups present in the VE resin was never the intention of the authors, as in previous studies done on the subject [92].

This part of the research was focused on the thermo-mechanical, morphological and optical effects produced by modifying the chemical composition of the copolymer phase. As aforementioned, the purpose of modifying the copolymer's composition by the addition of the monomer styrene (Figure 25), was to observe the effect that this modification had on some of the thermo-mechanical properties studied on Chapter II, such as modulus, glass transition temperature, transparency, molecular weight between crosslinks and fracture toughness. As it was explained in a previous chapter, some materials show the capacity to absorb energy from a ballistic impact by a deformation mechanism as a result of their ductility. This ductility is thought to be related to the molecular relaxation of side chain groups present in the chemical structure of the polymer. Side groups can affect the mobility of the polymer network when exposed to conditions where the rate of mechanical deformation increases reaching a threshold value [26].

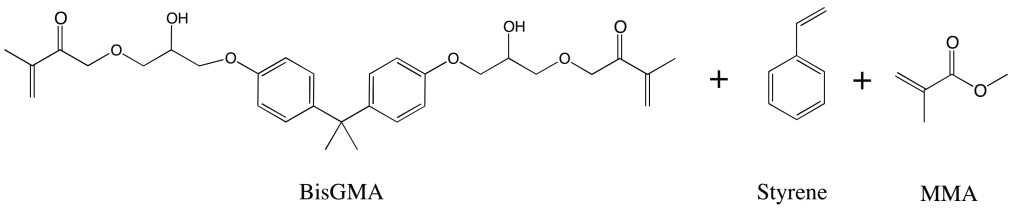

Figure 25. Modification of the copolymer phase by the addition of styrene.

MATERIALS and METHODS

Materials

Most of the reactants employed in this part of the research were the same used in chapter II. For the synthesis of the polyurethane phase (PU), two polyols were employed: 2-ethyl-2-(hydroxymethyl)-1,3propanediol (TRIOL) from Acros Organics, (USA)., and poly(tetramethylene ether) glycol (PTMG) average M_n ~ 650 and ~1400 g mol^{-1} from Sigma-Aldrich, (USA). The procedure to mix both polyols was the same used in chapter II. Where the TRIOL and PTMG mixture was melted in an oven under strong vacuum to remove moisture. The isocyanate used was hexamethylene diisocyanate 98.0% (DCH) from TCI, (USA). Two catalysts were used for the synthesis: dibutylin dilaurate, 98% (DD) distributed by Pfaltz & Bauer, (USA) and triphenylbismuth, 99+% (TB) from Alfa Aesar, (USA). Ethyl acetate was used as an analogue for both catalyzers.

The copolymer was synthetized using the bisphenol A bis(2-hydroxy-3-methacryloxypropyl) ether (BisGMA) from Esstech, (USA) and two acrylic monomers: methyl methacrylate 99% stabilized (MMA) from Alfa Aesar, (USA) and styrene 98% stabilized from Acros Orgnanics, (USA) while 2,2'-azobis(2-methylpropionitrile), 98% (AIBN) from Sigma-Aldrich, (USA) was used as an initiator.

Synthesis of graft-IPNs

The synthesis of the different styrene-based graft-IPN systems was carried out using the same procedure described in chapter II, where both the copolymer phase and the PU phase were prepared separately at room temperature conditions.

Several graft-IPN formulations were prepared for this study. The ratio of copolymer to polyurethane content changed from 90 wt% copolymer and 10 wt% PU to 60 wt% copolymer and 40 wt% PU, this was reproduced for the 650 and 1400 g mol^{-1} PTMG. The styrene content in the copolymer was change from 10 wt% to 90 wt%.

TECHNIQUES

Dynamic Mechanical Analysis

Dynamic mechanical analysis (DMA) on a TA Instruments RSA III was carried out to assess the thermo-mechanical properties by three-point bending. The tests were performed at temperatures ranging from 30 to 200 °C with a heating rate of 5 °C/min. The frequency was fixed a 1Hz and a sinusoidal strain-amplitude of 0.1 % was used for the analysis. The dynamic storage modulus (E′) and tan δ curves were plotted as a function of temperature. The temperature at the maximum in the tan δ curve was taken as the T_g.

Ultra violet Spectroscopy

As outline in Chapter II, UV- Vis transmittance spectra was collected for the various ratio of VE-based copolymer to 1400 g mol^{-1} PTMG based polyurethane, and with various amounts of styrene. All samples were analyzed in the 900-400 nm range.

Scanning Electron Microscopy

As outline in Chapter II, Scanning electron microscopy (SEM) was used to study the fracture surfaces of the 650 and 1400 g mol^{-1} PTMG based system, as well as for the study of samples with different styrene contents.

Fracture Toughness

As it was described in Chapter II, in order to characterize the fracture toughness of the graft-IPNs synthesized, in terms of the critical stress intensity factor, K_{IC}, quasi-static fracture tests were performed. The cured graft-IPN sheets were machined into rectangular coupons of dimensions 70 mm x 20 mm and 2.8 mm thickness in case of 650 g mol^{-1} PTMG VE-based graft-IPNs and 70 mm x 15 mm and 2.8 mm thickness for 1400 g mol^{-1} PTMG VE-based graft-IPNs. An edge notch of 3 mm in length was cut into the samples, and the notch tip was sharpened using a razor blade.

The load-deflection data was recorded up to crack initiation and during stable crack growth, if any. The crack initiation toughness or critical stress intensity factor, K_{IC}, was calculated

using the load (F) recorded at crack initiation. For each graft-IPN category, at least three sets of experiments were performed at laboratory conditions.

Tensile Analysis

To characterize the tensile properties of styrene-based graft-IPNs in terms of the elastic modulus, quasi-static tension tests were performed. For quasi-static tension tests, the cured styrene-base graft-IPN sheets were machined into dumbbell shaped specimen, which was inspired from ASTM D638 test method [70]. The size of the sheets that could be prepared precluded a complete adherence to ASTM standards. The load versus strain data was recorded up to 20 % strain for 650 and 1400 g mol^{-1} PTMG styrene-based graft-IPNs. Using the geometry of the specimen, stress was evaluated from load measurements to obtain stress versus strain data. For each styrene-graft-IPN category, at least three sets of experiments were performed at laboratory conditions. The elastic modulus was evaluated from the slope of the stress-strain curve at less than 2% strain.

RESULTS AND DISCUSSION

Thermo-mechanical characterization

In this chapter, the potential influence on the thermo-mechanical properties by modifying the chemical structure of the copolymer with the addition of styrene was assessed, as well as the effect of the molecular weight of poly (tetramethylene ether) glycol (PTMG).

From the dynamic mechanical analysis, it can be seen that the molecular weight of the PTMG for the synthesis of the graft-IPNs had a significant impact on the storage modulus depending

on the amount of styrene present in the system. However, it seems that only the ratio of copolymer to PU had a significant effect on the T_g of the systems. Figure 26, Figure 27 show the thermo-mechanical properties (storage modulus, E′, and tan δ) of the styrene-modified graft-IPNs synthesized using the 650 and 1400 g mol^{-1} PTMG as a function of temperature. While Figure 28 shows the thermo-mechanical properties of the styrene-modified graft-IPNs synthesized using different percentages of styrene in the copolymer as a function of temperature. In addition, Table 9 summarizes the results for all the different systems studied.

a)

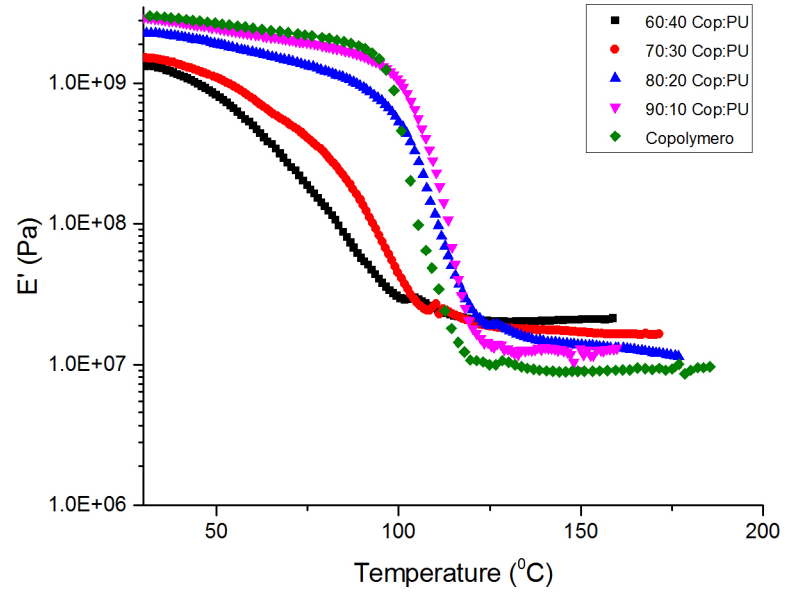

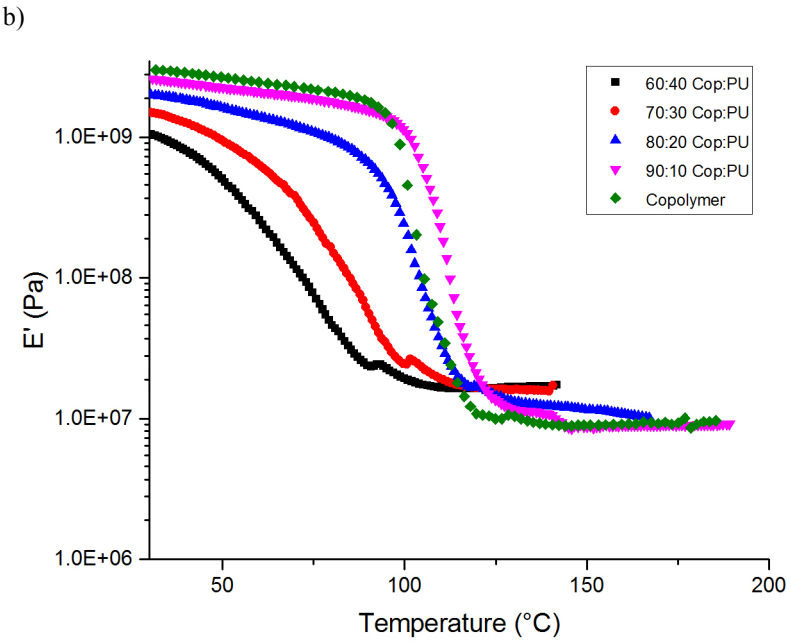

Figure 26. DMA results showing change in the storage modulus for styrene-modified graft-IPNs with various ratio of copolymer to (a) 650 g mol^{-1} PTMG based polyurethane and (b) 1400 g mol^{-1} PTMG based polyurethane. The copolymer was synthesized using 10 wt% of styrene.

For the styrene-modified graft-IPNs under study, it was observed that the storage modulus, E', increased as the weight percentage of copolymer increased, showing the same behavior as the graft-IPNs synthesized without styrene. Samples consisting of 90 wt% copolymer showed a storage modulus of 2.93, and 2.60 GPa at 30°C for the 650 and 1400 g mol^{-1} PTMG based styrene graft-IPNs. Samples under 80 wt% of copolymer exhibited far inferior values for the storage modulus. This behavior is attributed to the elastomeric contribution of the PU phase. When comparing the influence of the different molecular weight of the PTMGs, it can be seen that there is not an important difference in the storage modulus obtained for the two systems. As shown in Table 9, the storage modulus values for the system using the 1400 g mol^{-1} PTMG are mildly inferior to those of the 650 g mol^{-1}. This small difference cannot be attributed to the higher mobility that the 1400 g mol^{-1} provides to the PU network, as it was

stated for the MMA copolymer based graft-IPNs, where a substantial difference between systems was observed [62]. Figure 27 a) and b), show the plot of tan δ as a function of temperature for the styrene-based graft-IPNs synthesized using the 650 and 1400 g mol^{-1} PTMG.

b)

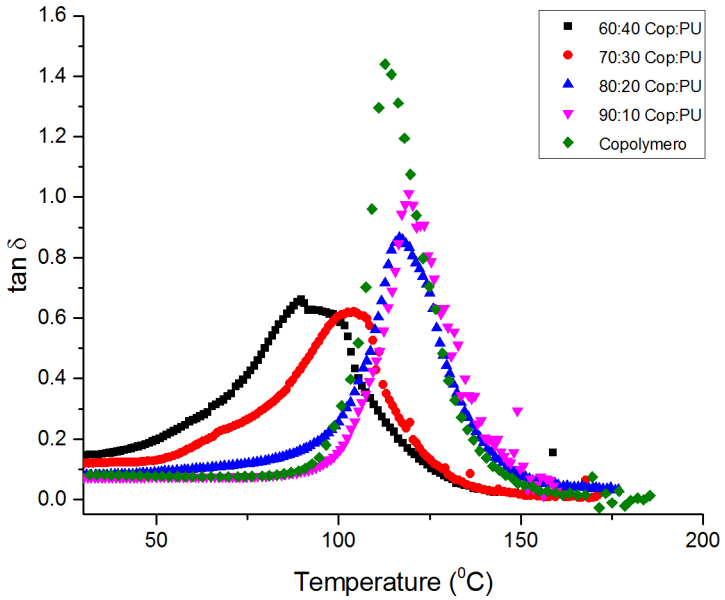

b)

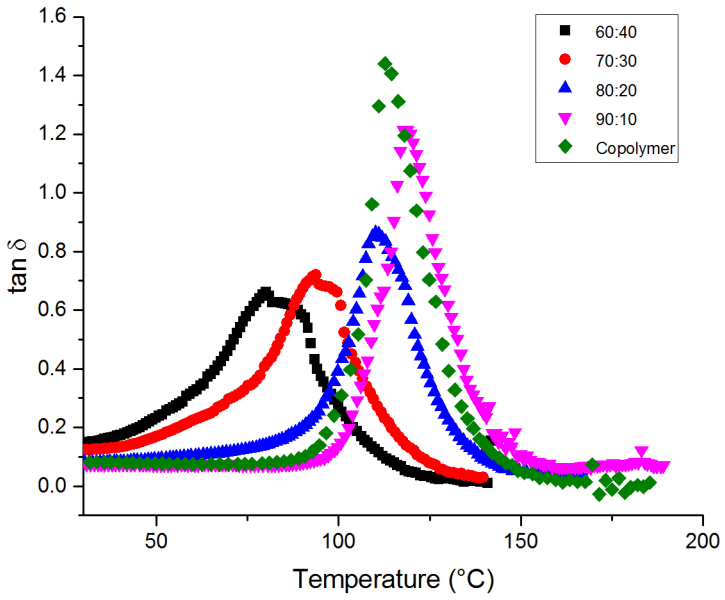

Figure 27. DMA results showing change in tan δ for graft-IPNs with various ratio of styrene-based copolymer to a) 650 g mol^{-1} PTMG based polyurethane, and b) 1400 g mol^{-1} PTMG based polyurethane

In Figures 27 a) and b), the maximum peak of the loss factor showed the characteristic relaxation associated with the glass transition temperature of the different styrene-modified graft-IPNs under study. It was observed that as the weight percentage of copolymer increased in the samples, the maximum peak of the loss factor gained prominence and moved to higher temperatures. This tendency was also observed for the MMA-based copolymer graft-IPNs. However, for the styrene-modified graft-IPNs systems, it seems that the addition of styrene in the system affects the mobility of the network, thus, reducing its glass transition temperature [93]. This can be more easily seen in the copolymer sample, where it clearly showed a glass transition temperature below the one showed by the 90 % copolymer sample. This phenomenon can be observed for both the 650 and 1400 g mol^{-1} PTMG based systems.

Samples with a copolymer composition below 80 wt% showed broad transitions with a slight shoulder related to the glass transition of the polyurethane rubbery phase; characteristic of a partially miscible system. On the other hand, samples with a copolymer content above 70 wt% presented a narrow peak for the loss factor, which as discussed in a previous chapter, this narrow peak suggests an elevated degree of miscibility between the components. An almost identical behavior was also observed for the composition using the 1400 g mol^{-1} PTMG. These broad transitions observed for the styrene-modified graft-IPNs are related to the many different relaxation mechanisms that are present in the synthesized network, as a results of the nano-heterogeneity displayed by the system [53, 62]. Figure 28 shows the

storage modulus for samples with a copolymer to PU ratio of 70:30 and increasing content of styrene in the copolymer phase.

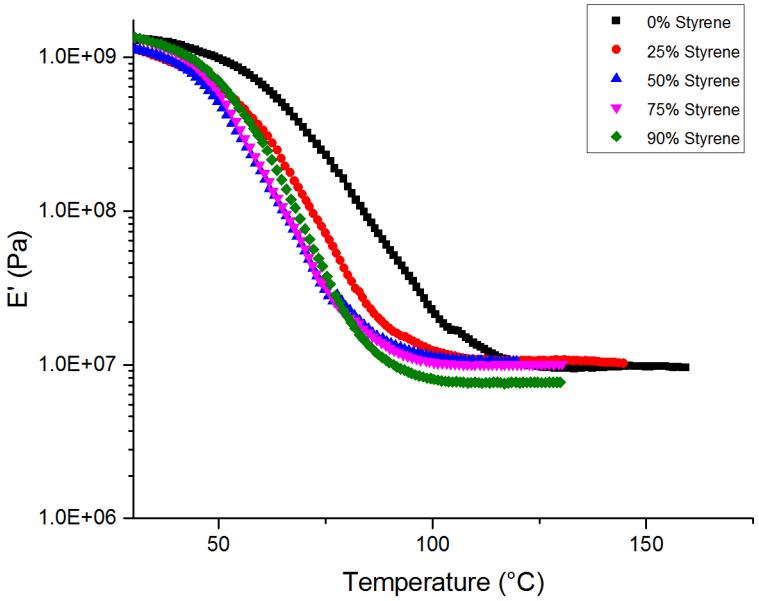

Figure 28. DMA results showing change in the storage modulus for styrene-modified graft-IPNs with various amounts of styrene with the 1400 g mol^{-1} PTMG based polyurethane.

In order to isolate and analyze the effect of adding styrene to the copolymer phase on the thermo-mechanical properties of the system, several different formulations were prepared with an increasing amount of styrene in the copolymer phase, while keeping the same molecular weight of PTMG for the polyurethane phase, which for this test the 1400 g mol^{-1} was selected. From Table 9, it can be seen that an increasing amount of styrene in the copolymer phase had little effect on the storage modulus, E', of the styrene-modified graft-IPN systems. Moreover, when compared to its MMA copolymer-based graft-IPN counterpart, it can be seen that the values for the storage modulus are really similar to each other. This is an unexpected result, since the styrene-based graft-IPNs presented lower glass transitions values compared to those displayed by the MMA copolymer-based graft-IPNs. Figure 29,

shows the plot of tan δ as a function of temperature for the styrene-based graft-IPNs synthesized using the 1400 g mol^{-1} PTMG and various amount of styrene in the copolymer phase.

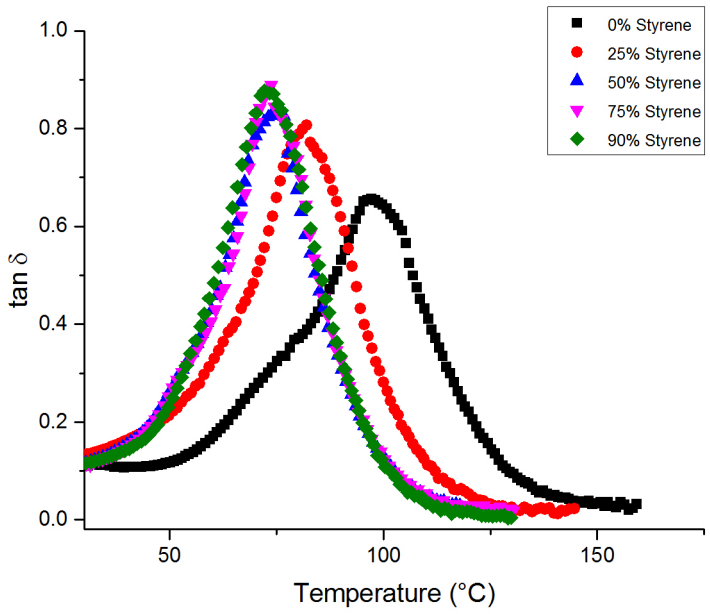

Figure 29. DMA results showing change in tan δ for graft-IPNs with 1400 g mol^{-1} PTMG based polyurethane and various amount of styrene present in the copolymer.

As it can be seen on Figure 29, an increment on the amount of styrene present on the samples seems to not have a significant impact on the glass transition temperature of the system. The sample containing 25 wt% of styrene seems to be the only one that deviates from the rest, showing a slightly higher glass transition temperature. From Figure 29, one can notice how samples with styrene in their composition showed a less broad transition when compare to the MMA copolymer-based graft-IPN, what may suggest that the styrene-based graft-IPNs present a higher degree of miscibility that their MMA counterparts. When comparing all the styrene-based graft-IPNs analyzed on this section, it seems that the best combination of

storage modulus and glass transition temperature is achieved by adding 10 wt% of styrene to the copolymer phase and using a 650 g mol^{-1} PTMG base polyurethane.

Table 9. Storage modulus, E′, glass transition temperature, T_g, for the different styrene-based graft-IPNs synthesized.

Sample	Copolymer content (wt%)	Styrene content (wt%)	E′ (Pa) at 30 °C	T_g (°C)
VE-graft-IPN with 650 g mol^{-1} PTMG	100	10	3.01×10^9	112
	90	10	2.93×10^9	119
	80	10	2.26×10^9	117
	70	10	1.52×10^9	104
	60	10	1.32×10^9	92
Graft-IPN with 1400 g mol^{-1} PTMG	100	10	3.01×10^9	112
	90	10	2.60×10^9	118
	80	10	2.00×10^9	110
	70	10	1.51×10^9	94
	60	10	1.05×10^9	80
VE-graft-IPN with 1400 g mol^{-1} PTMG	70	90	1.35×10^9	72
	70	75	1.35×10^9	74
	70	50	1.13×10^9	75
	70	25	1.12×10^9	82

Degree of transparency

The degree of transparency of the styrene-based graft-IPNs was analyzed. Figure 30 shows the percentage of transmittance as a function of wavelength for set of samples with a copolymer to polyurethane ratio of 70:30 and various amounts of styrene present in the copolymer. For this set of samples the PTMG use for the synthesis of the polyurethane phase

was the 1400 g mol^{-1}. As it can be seen from Figure 30, samples with a styrene content below 90% exhibited transmittance values between 70 and 85 percent.

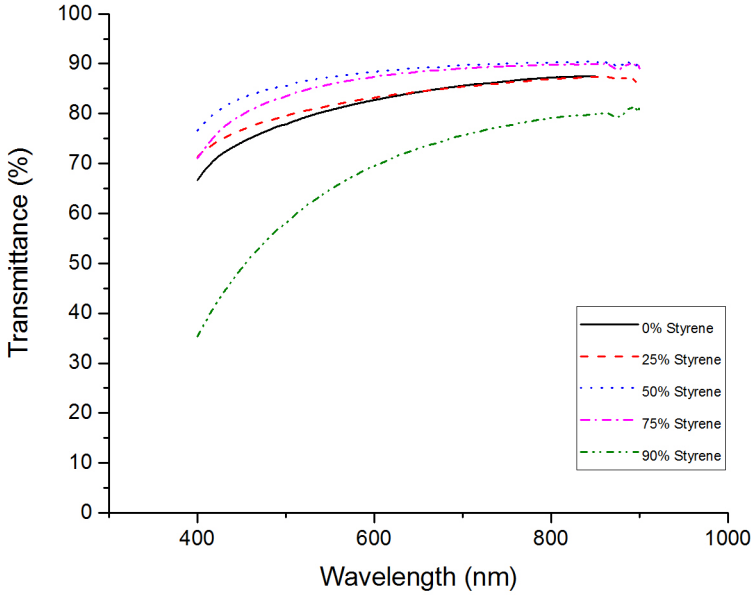

Figure 30. UV-vis spectrum of styrene-based copolymer and 1400 g mol^{-1} PTMG based polyurethane graft-IPN, with increasing amounts of styrene in the copolymer.

Figure 31, shows the percentage of transmittance as a function of wavelength for samples with different copolymer to polyurethane ratios and 10 wt% of styrene in the copolymer. The 1400 g mol^{-1} was use for the synthesis of the rubbery phase. From Figure 31 one can see how the transmittance values for samples with a copolymer content below 80% are severely affected by the increasing amount of the rubbery phase. When compare to their MMA copolymer based graft-IPNs counterparts this behavior was not observed. This may be the result of some degree of phase separation present in the samples analyzed.

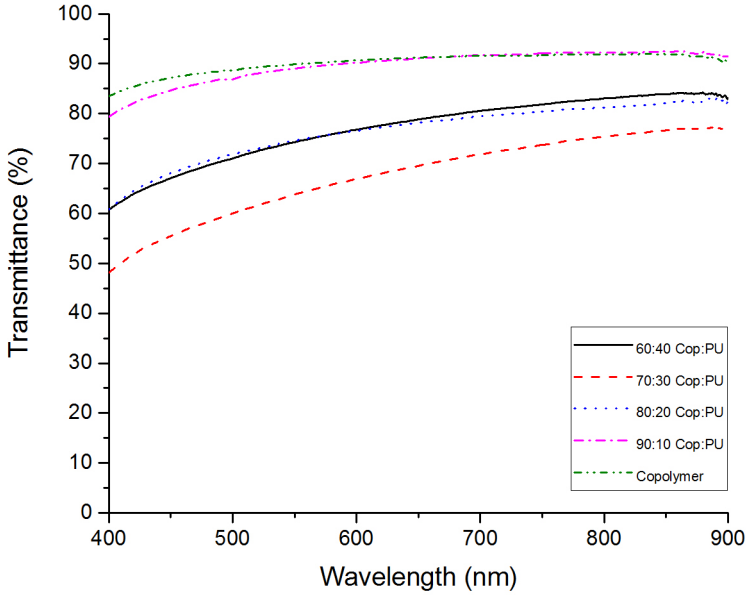

Figure 31. UV-vis spectrum of styrene-based copolymer and 1400 g mol^{-1} PTMG based polyurethane graft-IPN, with 10 wt% of styrene present in the copolymer.

These results suggest that the styrene-based graft-IPNs show a relatively high degree of interpenetration. As in the case of their non-styrene graft-IPNs, the system with increasing amount of styrene shows no visible evidence of a macroscopic phase separation. This results support the high degree of miscibility observed in the plot of tan δ as a function of temperature.

Stiffness and fracture toughness

The stress versus strain plots obtained from the tension tests in case of 650 and 1400 g mol^{-1} PTMG are shown in Figure 32 a) and b) respectively. These results were obtained from Dr. Tippur's research group in the Department of Mechanical Engineering at Auburn University, Alabama. One can see that the modulus and the peak stress drops progressively for all samples under analysis. However, as in the case of the MMA-based graft-IPNs synthesized

using the 1400 g mol^{-1} PTMG, all styrene-based graft-IPNs presented the same behavior were no failure was observed within the window of imposed strains.

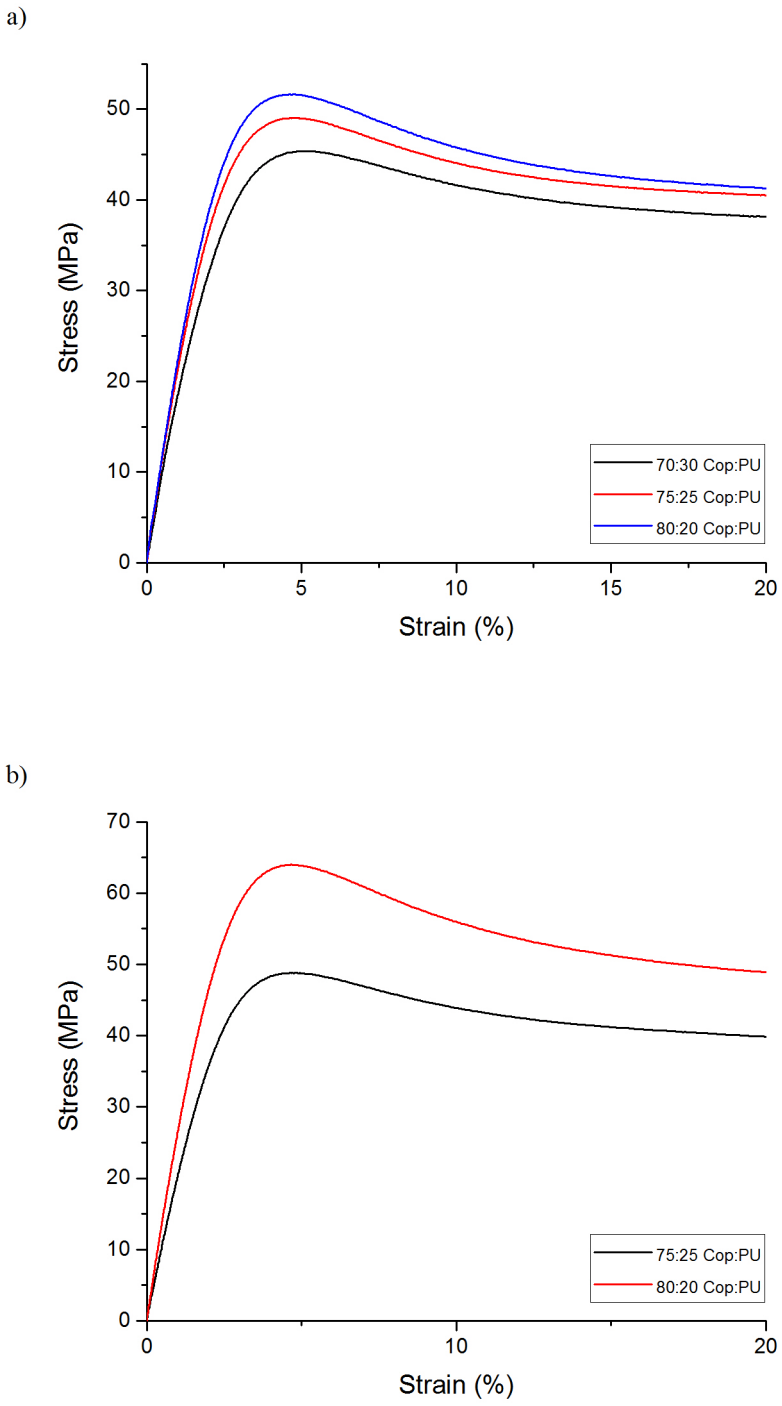

Figure 32. Stress versus Strain plots for styrene-based copolymer samples using (a) 650 g mol^{-1} PTMG and (b) 1400 g mol^{-1} PTMG based polyurethane during tension test.

Table 10 shows results obtained for the quasi-static crack initiation toughness, K_{IC} for the styrene-based graft-IPNs under studied. When comparing the different systems, it can be seen that the styrene-based graft-IPNs synthesized using the 650 g mol^{-1} PTMG presented a slightly higher value for the quasi-static crack initiation toughness than those with a 1400 g mol^{-1} PTMG based polyurethane phase. Moreover, it can be seem that the highest value of fracture toughness displayed by the styrene-based graft-IPNs corresponds to the sample with a 70% of copolymer content. This was the same composition that showed the highest fracture toughness for the MMA-based graft-IPNs. This serves as a confirmation that there is an optimum copolymer to PU ratio in order to achieve the best fracture properties.

Table 10. Results obtained for the fracture toughness tests performed on different styrene-based graft-IPNs synthesized with 10 wt% of styrene in the copolymer phase.

Sample	Copolymer content (wt%)	K_{Ic} (MPa $m^{1/2}$)	E (GPa)	Failure strain (%)
Graft-IPN with 650 g/mol PTMG	80	1.60 ±0.209	2.86±0.05	>20
	75	2.35 ±0.213	2.78±0.03	>20
	70	3.30 ±0.202	2.06±0.02	>20
Graft-IPN with 1400 g/mol PTMG	80	1.25 ±0.05	2.94±0.05	>20
	75	2.25 ±0.08	2.34±0.05	>20
	70	--	--	--

Surface Morphology

In order to compare the fracture mechanics of the styrene-based graft-IPN with different molecular weight PTMGs and different styrene content in the copolymer, SEM images were taken. The samples compared had a copolymer to polyurethane ratio of 70:30, as in previous experiments, the different molecular weight PTMG employed for the synthesis of the polyurethane phase were the 650 and 1400 g mol^{-1}, and the styrene content was changed between 10 and 45 wt%. Figure 33 shows the fractured surfaces of styrene-based graft-IPNs.

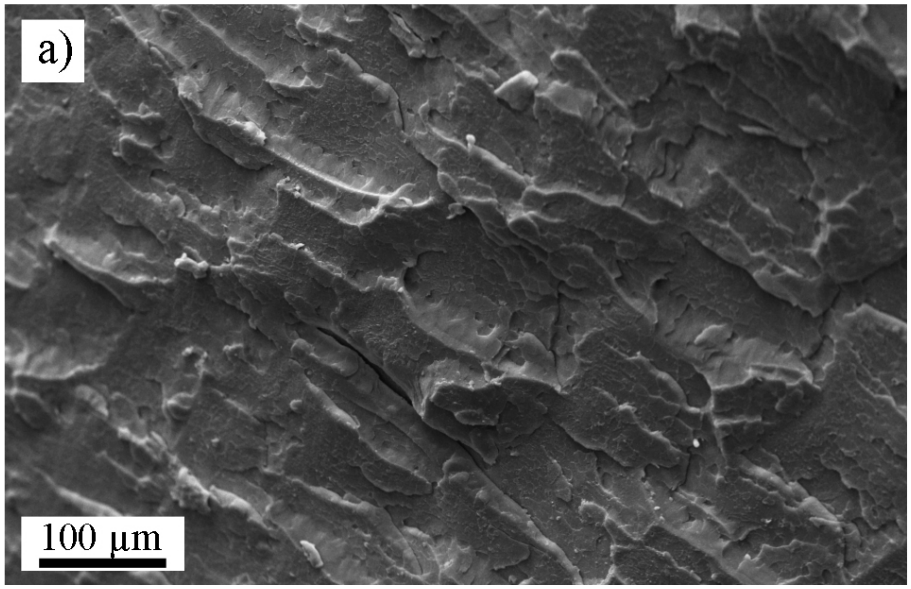

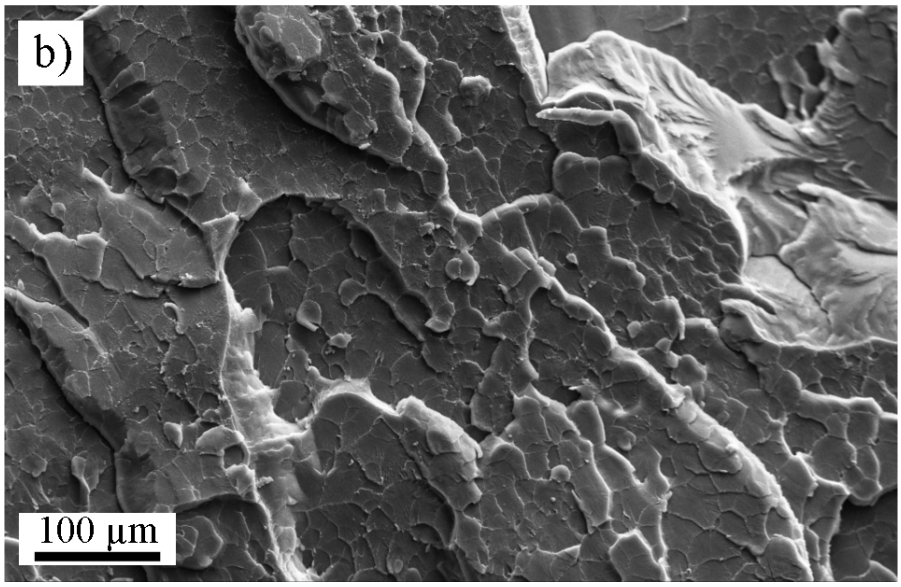
b)
100 µm

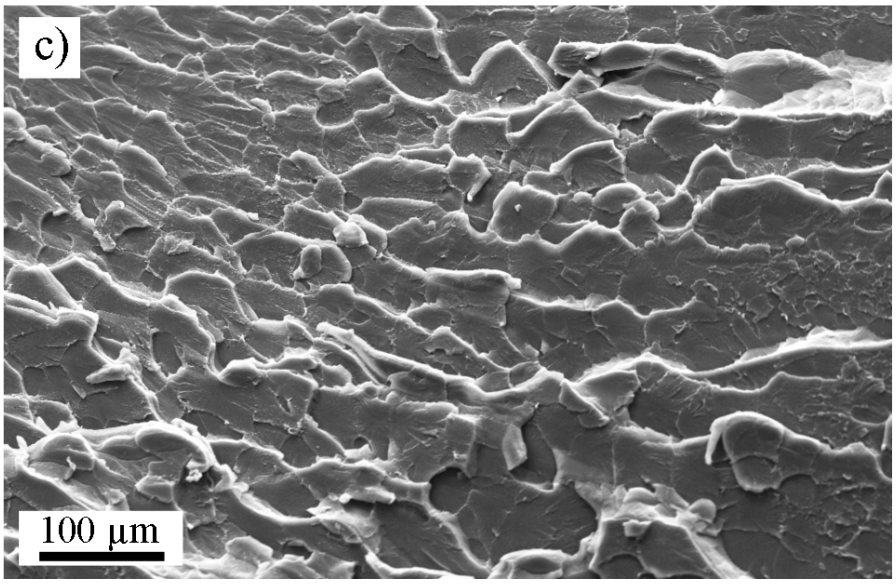
c)
100 µm

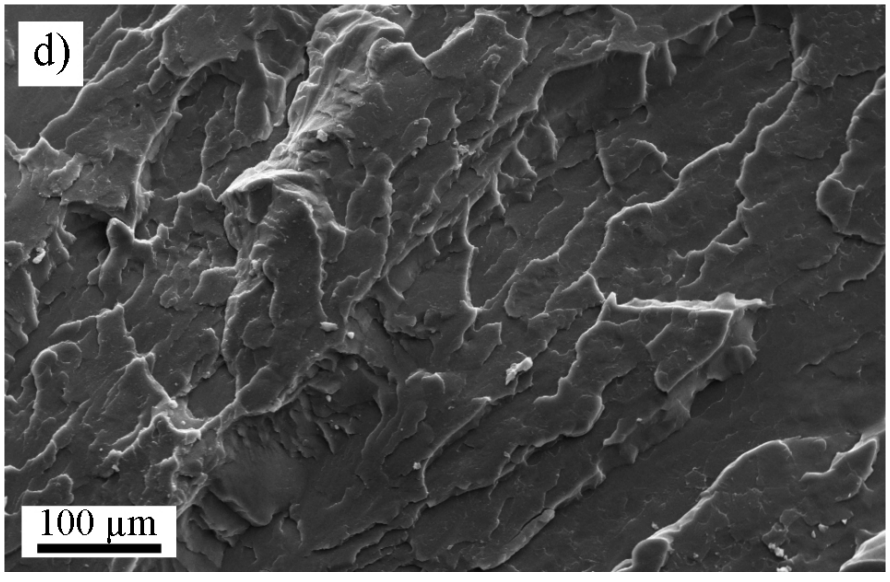
d)
100 µm

Figure 33. SEM photos of (a) 650 g mol^{-1} PTMG based polyurethane and 10 wt% of styrene, and (b) 1400 g mol^{-1} PTMG based polyurethane and 10 wt% of styrene, (c) 650 g mol^{-1} PTMG based polyurethane and 45 wt% of styrene, and (d) 1400 g mol^{-1} PTMG based polyurethane and 45 wt% of styrene VE-based graft-IPNs.

From Figure 33 it can be seen that regardless of the molecular weight of the PTMG employed for the synthesis of the polyurethane phase, this variable seems to not have a major impact on the surface area generated by the propagation of the fracture. The same result was also observed when the styrene content was increased from 10 to 45 wt% in the copolymer phase. When compared to their non-styrene counterparts, one can see the similarities of the surface area generated were the fracture propagated through the material. One can speculate that the styrene-based graft-IPNs possess a similar fracture mechanism responsible for the energy absorption as their non-styrene counterparts.

CONCLUSIONS

In this chapter, different styrene-based graft-IPNs were synthesized. Here, the copolymer phase was chemically modified by a adding a third monomer (styrene). This chapter focused on studying the influence of adding this new monomer on the thermo-mechanical and fracture toughness properties of the final material. Other variables studied include: the influence of the copolymer to PU ratio, molecular weight of the PTMG, as well as both network and surface morphology.

As in a previous chapter, it was found that the toughenability of the styrene-based graft-IPNs was affected by the molecular weight of the PTMG employed, the copolymer to PU ratio used as well as for the chemical modification of the copolymer by the addition of the styrene monomer. The styrene-based graft-IPNs synthesized showed a similar behavior to those of their non-styrene based graft-IPNs. These styrene-modified graft-IPNs displayed the highest fracture toughness values when the sample had a 30% of polyurethane content and when a 10 wt% of styrene monomer was present in the copolymer's composition. Moreover, the addition of just 10% of styrene in the copolymer had an improvement on the fracture toughness of 22%, when compared to the same samples without styrene. The addition of styrene also seems to improve the miscibility of the graft-IPNs systems. However, it was observed that the addition of the styrene monomer had the tendency to lower the glass transition temperature of the systems. The surface morphology analysis suggests that the styrene-based graft-IPNs follow the same fracture mechanism that is accountable for the improvement in the fracture toughness, when compared to their non-grafted counterparts.

FUTURE WORK

In order to further understand the stress relaxation mechanisms present in all the different graft-IPNs systems, it is most important to analyze the stress relaxation behavior of the copolymer phase when this networks is modified by the addition of a third monomer. The influence of the inclusion of a third monomer into the chemical structure of the backbone of the polymer chain as well as the effect of its concentration in the network needs to be addressed in future analysis. The understanding of the molecular dynamics of the graft-IPNs could shed some light on some of the improvements on the mechanical properties of the graft-IPNs over their non-grafted counterparts.

In the case of the styrene-based graft-IPNs it is highly important to study the triblock copolymer's parameters that control the morphology and the mechanical properties. Transmission electron microscope imaging is highly important to understand how the chemical structure of the triblock copolymer affects the network morphology as well as the surface morphology of the styrene-based graft-IPNs. It is also important to perform aging studies on the materials, since the ability of withstanding harsh environmental conditions is a highly important requirement for the application of these materials in both military and civilian applications.

REFERENCES

1. Lucy Rodgers, David Gritten, James Offer, and Patrick Asare, "Syria: The story of the conflict," BBC news, October 9, 2015, accessed October 17, 2015, http://www.bbc.com/news/world-middle-east-26116868.

2. Fischer, Hannah. 2015. "A Guide to U . S . Military Casualty Statistics : Operation Freedom ' S Sentinel , Operation Inherent Resolve , Operation New Dawn , Operation Iraqi Freedom , and Operation Enduring Freedom."

3. Grujicic, M., B. Pandurangan, N. Coutris, B.A. Cheeseman, C. Fountzoulas, P. Patel, and Elmar Strassburger. 2008. "A Ballistic Material Model for Starphire®, a Soda-Lime Transparent-Armor Glass." *Materials Science and Engineering: A* 491 (1-2): 397–411. doi:10.1016/j.msea.2008.02.020.

4. Grujicic, M., W. C. Bell, and B. Pandurangan. 2012. "Design and Material Selection Guidelines and Strategies for Transparent Armor Systems." *Materials and Design* 34: 808–819. doi:10.1016/j.matdes.2011.07.007.

5. Active NIJ Standards and Comparative Test Methods. 2012. Cited 2015; Available from: http://www.nij.gov/topics/technology/standards-testing/active.htm.

6. US Army purchase specification. ATPD-2352; 2008.

7. Klement, R., S. Rolc, R. Mikulikova, and J. Krestan. 2008. "Transparent Armour Materials." *Journal of the European Ceramic Society* 28 (5): 1091–1095. doi:10.1016/j.jeurceramsoc.2007.09.036.

8. Hazell, P.J., M.R. Edwards, H. Longstaff, and J. Erskine. 2009. "Penetration of a Glass-Faced Transparent Elastomeric Resin by a Lead–antimony-Cored Bullet." *International Journal of Impact Engineering* 36 (1) (January): 147–153. doi:10.1016/j.ijimpeng.2007.12.009.

9. Antoine, G.O., and R.C. Batra. 2015. "Optimization of Transparent Laminates for Specific Energy Dissipation under Low Velocity Impact Using Genetic Algorithm." *Composite Structures* 124: 29–34. doi:10.1016/j.compstruct.2014.12.066.

10. James M. Sands, Parimal J. Patel, Peter G. Dehmer, Alex J. Hsieh, and Mary C. Boyce. 2004. "Protecting the Future Force: Transparent Materials Safeguard the Army's Vision," AMPTIAC Quaterly, Volume 8, Number 4 (28-36).

11. Tasdemirci, a., G. Tunusoglu, and M. Güden. 2012. "The Effect of the Interlayer on the Ballistic Performance of Ceramic/composite Armors: Experimental and Numerical Study." *International Journal of Impact Engineering* 44: 1–9. doi:10.1016/j.ijimpeng.2011.12.005.

12. Wang, Qun, Zhaohai Chen, and Zhaofeng Chen. 2013. "Design and Characteristics of Hybrid Composite Armor Subjected to Projectile Impact." *Materials & Design* 46: 634–639. doi:10.1016/j.matdes.2012.10.052.

13. Öberg, E K, J Dean, and T W Clyne. 2015. "Effect of Inter-Layer Toughness in Ballistic Protection Systems on Absorption of Projectile Energy." *International Journal of Impact Engineering* 76: 75–82. doi:10.1016/j.ijimpeng.2014.09.006.

14. Medvedovski, Eugene. 2010. "Ballistic Performance of Armour Ceramics: Influence of Design and Structure. Part 1." *Ceramics International* 36 (7): 2103–2115. doi:10.1016/j.ceramint.2010.05.021.

15. Mel Schwartz, Innivations in Materials Manufacturing, Fabrication, and Environmental Safety (Florida: CRC Press, 2011), 461-464.

16. Grujicic, M., W. C. Bell, B. Pandurangan, B. a. Cheeseman, C. Fountzoulas, and P. Patel. 2012. "Molecular-Level Simulations of Shock Generation and Propagation in Soda-Lime Glass." *Journal of Materials Engineering and Performance* 21 (8): 1580–1590. doi:10.1007/s11665-011-0064-4.

17. Shim, Gyu-In, Seong-Hwan Kim, Hyeng-Woo Eom, Deok-Lae Ahn, Jong-Kyoo Park, and Se-Young Choi. 2015. "Improvement in Ballistic Impact Resistance of a Transparent Bulletproof Material Laminated with Strengthened Soda-Lime Silicate Glass." *Composites Part B: Engineering* 77: 169–178. doi:10.1016/j.compositesb.2015.03.035.

18. Edgar D. Zanotto. 2000. "Abright future for glass-ceramics." American Ceramic Society Bulletin, Volume 89, Number 8 (19-27).

19. Haney, Edward J., and Ghatu Subhash. 2011a. “Analysis of Interacting Cracks due to Sequential Indentations on Sapphire.” *Acta Materialia* 59 (9): 3528–3536. doi:10.1016/j.actamat.2011.02.026.

20. Haney, Edward J., 2011b. “Static and Dynamic Indentation Response of Basal and Prism Plane Sapphire.” *Journal of the European Ceramic Society* 31 (9): 1713–1721. doi:10.1016/j.jeurceramsoc.2011.03.006.

21. Liu, X.J., F. Chen, F. Zhang, H.L. Zhang, Z. Zhang, J. Wang, S.W. Wang, and Z.R. Huang. 2013. “Hard Transparent AlON Ceramic for visible/IR Windows.” *International Journal of Refractory Metals and Hard Materials* 39: 38–43. doi:10.1016/j.ijrmhm.2013.01.021.

22. Luo, Zhiwei, Gao Qu, Yuhua Zhang, Lei Cui, and Anxian Lu. 2013. “Transparent Oxynitride Glasses: Synthesis, Microstructure, Optical Transmittance and Ballistic Resistance.” *Journal of Non-Crystalline Solids* 378: 45–49. doi:10.1016/j.jnoncrysol.2013.06.011.

23. Su, Mingyi, Youfu Zhou, Kun Wang, Zhangfu Yang, Yongge Cao, and Maochun Hong. 2015. “Highly Transparent AlON Sintered from Powder Synthesized by Direct Nitridation.” *Journal of the European Ceramic Society* 35 (4): 1173–1178. doi:10.1016/j.jeurceramsoc.2014.10.036.

24. Kim, Jin-Myung, Ha-Neul Kim, Young-Jo Park, Jae-Woong Ko, Jae-Wook Lee, and Hai-Doo Kim. 2015. “Fabrication of Transparent MgAl2O4 Spinel through Homogenous Green Compaction by Microfluidization and Slip Casting.” *Ceramics International* 41 (10): 13354–13360. doi:10.1016/j.ceramint.2015.07.121.

25. Straßburger, E. 2009. “Ballistic Testing of Transparent Armour Ceramics.” *Journal of the European Ceramic Society* 29 (2): 267–273. doi:10.1016/j.jeurceramsoc.2008.03.049.

26. Patel, Parimal J, Alex J Hsieh, Gary A Gilde, and Aberdeen Proving Ground. 2004. "IMPROVED LOW-COST MULTI-HIT TRANSPARENT ARMOR Report Documentation Page."

27. Kim, C.S., and S.M. Oh. 2002. "Spectroscopic and Electrochemical Studies of PMMA-Based Gel Polymer Electrolytes Modified with Interpenetrating Networks." *Journal of Power Sources* 109 (1): 98–104. doi:10.1016/S0378-7753(02)00055-1.

28. Hakimelahi, Hamid R., Ling Hu, Bradley B. Rupp, and Maria R. Coleman. 2010. "Synthesis and Characterization of Transparent Alumina Reinforced Polycarbonate Nanocomposite." *Polymer* 51 (12): 2494–2502. doi:10.1016/j.polymer.2010.04.023.

29. Yeqiu, Liu, Hu Jinlian, Zhu Yong, and Yang Zhuohong. 2005. "Surface Modification of Cotton Fabric by Grafting of Polyurethane." *Carbohydrate Polymers* 61 (3): 276–280. doi:10.1016/j.carbpol.2005.03.010.

30. L. H. Sperling, Introduction to Physical Polymer Science. (Hoboken: John Wiley & Sons, Inc, 2006), 687-693.

31. L. H. Sperling, and V. Mishra. "The current Status of Interpenetrating Polymer Networks." Polymers for Advanced Technologies (7): 197-208.

32. Mohammadi, H., and N. Mohammadi. 2012. "Fracture of Polymer Blends: Effect of Characteristic Number of Interfacial Entanglements and Matrix Toughness." *Polymer (United Kingdom)* 53 (13): 2769–2776. doi:10.1016/j.polymer.2012.04.034.

33. Sivaraman, P., N.R. Manoj, V.S. Mishra, R.D. Raut, a.B. Samui, and B.C. Chakraborty. 2005. "Thermoplastic Copolyether Ester Elastomer Toughened Polycarbonate Blends 3. Microhardness and Abrasion Resistance of the Blends." *Polymer Testing* 24 (2): 241–243. doi:10.1016/j.polymertesting.2004.07.006.

34. Ma, Wen Yan, Yi Xian Wu, Li Feng, and Ri Wei Xu. 2012. "Synthesis of Poly(styrene-Co-Isopropenyl Acetate) -G-Polyisobutylene Graft Copolymers via Combination of Radical Polymerization with Cationic Polymerization." *Polymer (United Kingdom)* 53 (15): 3185–3193. doi:10.1016/j.polymer.2012.05.028.

35. Jouenne, Stéphane, Juan a. González-Léon, Anne-Valérie Ruzette, Philippe Lodéfier, and Ludwik Leibler. 2008. “Styrene−Butadiene Gradient Block Copolymers for Transparent Impact Polystyrene.” *Macromolecules* 41 (24): 9823–9830. doi:10.1021/ma801327x.

36. Lach, R, R Adhikari, R Weidisch, T A Huy, G H Michler, W Grellmann, and K Knoll. 2004. “Crack Toughness Behavior of Binary Poly(styrene-Butadiene) Block Copolymer Blends.” *Journal of Materials Science* 39 (4): 1283–1295. doi:10.1023/B:JMSC.0000013887.79570.33.

37. Cureton, LaShonda T., and S. Richard Turner. 2011. “Synthesis and Properties of Bisphenol A–terphenol Poly(arylene Ether Sulfone)–polydimethylsiloxane Segmented Block Copolymers.” *European Polymer Journal* 47 (12): 2303–2310. doi:10.1016/j.eurpolymj.2011.09.006.

38. Tamai, Toshikazu, Akira Imagawa, Qui Tran-cong, Received February, Revised Manuscript, and Received September. 1994. “Semi-Interpenetrating Polymer Networks Prepared by” (November): 7486–7489.

39. Tadao. Kotaka, Shiro. Nishi, and Hiroshi. Adachi. “Sequential Interpenetrating Polymer Networks: Synthesis, Structure, and Properties.” Advances in Interpenetrating Polymer Networks, ed. D. Klempner and K. C. Frisch. Vol. 2. 1990, Lancaster: Techonomic Publishing Company, Inc.

40. Sperling, L H. 1994. “Interpenetrating Polymer Networks : An Overview.” *Materials Science*: 3–38. doi:10.1021/ba-1994-0239.

41. Lav, Thanh-Xuan, Benjamin Carbonnier, Mohamed Guerrouache, and Daniel Grande. 2010. “Porous Polystyrene-Based Monolithic Materials Templated by Semi-Interpenetrating Polymer Networks for Capillary Electrochromatography.” *Polymer* 51 (25): 5890–5894. doi:10.1016/j.polymer.2010.10.032.

42. B. Y. Li, X. P. Bi, D. H. Zhang, and F. S. Wang. “Forced Compatibility and Mutual Entanglements in Poly(Vinyl Acetate)/Poly(Methyl Acrylate) IPNs.” Advances in Interpenetrating Polymer Networks, ed. D. Klempner and K. C. Frisch. Vol. 1. 1989, Lancaster: Techonomic Publishing Company, Inc.

43. B. J. P. Jansen, S. Rastogi, H. E. M. Meijer, and P. J. Lemstra. 1999. "Rubber-Modified Glassy Amorphous Polymers Prepared via Chemically Induced Phase Separation. 4. Comparison of Properties of Semi-and Full-IPNs, and Copolymers of Acrylate-Aliphatic Epoxy Systems." Macromolecules (32): 6290-6297.

44. Yu, Haibo, Jing Peng, Maolin Zhai, Jiuqiang Li, Genshuan Wei, and Jinliang Qiao. 2007. "Synthesis and Characterization of Poly (n-Butyl Acrylate)-Poly (methyl Methacrylate) Latex Interpenetrating Polymer Networks by Radiation-Induced Seeded Emulsion Polymerization." *Radiation Physics and Chemistry* 76 (11-12): 1746–1750. doi:10.1016/j.radphyschem.2007.02.088.

45. Shi, S, S Kuroda, S Tadaki, and H Kubota. 2002. "Phase Distribution and Separation in Poly (2-Acetoxyethyl Methacrylate)/ Polystyrene Latex Interpenetrating Polymer Networks" 43: 7443–7450.

46. Yu. S. Lipatov, and L. V. Karabanova. "Gradient Interpenetrating Polymer Networks." Advances in Interpenetrating Polymer Networks, ed. D. Klempner and K. C. Frisch. Vol. 4. 1994, Lancaster: Techonomic Publishing Company, Inc.

47. G. C. Berry, and M. Dror. 1978. Am. Chem. Soc. Div. Org. Coat Plast. Prepr., 38:465.

48. Bastani, Saeid, and Siamak Moradian. 2006. "UV-Curable Powder Coatings Containing Interpenetrating Polymer Networks (IPNs)." *Progress in Organic Coatings* 56 (2-3): 248–251. doi:10.1016/j.porgcoat.2005.06.014.

49. Dean, K., W. D. Cook, P. Burchill, and M. Zipper. 2001. "Curing Behaviour of IPNs Formed from Model VERs and Epoxy Systems: Part II. Imidazole-Cured Epoxy." *Polymer* 42 (8): 3589–3601. doi:10.1016/S0032-3861(00)00745-X.

50. Dragan, Ecaterina Stela. 2014. "Design and Applications of Interpenetrating Polymer Network Hydrogels. A Review." *Chemical Engineering Journal* 243 (MAY 2014): 572–590. doi:10.1016/j.cej.2014.01.065.

51. Yin, Z.N., and T.J. Wang. 2010. "Deformation Response and Constitutive Modeling of PC, ABS and PC/ABS Alloys under Impact Tensile Loading." *Materials Science*

and Engineering: A 527 (6): 1461–1468. doi:10.1016/j.msea.2009.11.025.

52. Gao, Jianing, Junting Li, Su Zhao, Brian C. Benicewicz, Henrik Hillborg, and Linda S. Schadler. 2013. "Effect of Graft Density and Molecular Weight on Mechanical Properties of Rubbery Block Copolymer Grafted SiO2 Nanoparticle Toughened Epoxy." *Polymer* 54 (15) (July): 3961–3973. doi:10.1016/j.polymer.2013.05.033.

53. Bird, SA, D Clary, and KC Jajam. 2013. "Synthesis and Characterization of High Performance, Transparent Interpenetrating Polymer Networks with Polyurethane and Poly (methyl Methacrylate)." *Polymer Engineering ...*: 1–8. doi:10.1002/pen.

54. Pfeifer C. S., Silva L. R., Kawano Y., Braga R. R.: Bis-GMA co-polymerizations: Influence on conversion, flexural properties, fracture toughness and susceptibility to ethanol degradation of experimental composites. Dental Materials*:* Official Publication of the Academy of Dental Materials, 25, 1136–41 (2009). DOI: 10.1016/j.dental.2009.03.010.

55. Mulliken A. D., Boyce M. C.: Mechanics of the rate-dependent elastic–plastic deformation of glassy polymers from low to high strain rates. International Journal of Solids and Structures, 43, 1331–1356 (2006). DOI: 10.1016/j.ijsolstr.2005.04.016.

56. Panapitiya N. P., Wijenayake S. N., Huang Y., Bushdiecker D., Nguyen D., Ratanawanate C., Kalaw G. J., Gilpin C. J., Musselman I. H., Balkus K. J., Ferraris J. P.: Stabilization of immiscible polymer blends using structure directing metal organic frameworks (MOFs). Polymer, 55, 2028–2034 (2014). DOI: 10.1016/j.polymer.2014.03.008.

57. Sperling L. H.: Polymeric Multicomponent Materials: An Introduction. Wiley-Interscience, New York (1997).

58. Mignard N., Okhay N., Jegat C., Taha M.: Facile elaboration of polymethylmethacrylate/polyurethane interpenetrating networks using Diels-Alder reactions. Journal of Polymer Research, 20:233 (2013). DOI: 10.1007/s10965-013-0233-2.

59. Cerclé C., Favis B. D.: Generalizing Interfacial Modification in Polymer Blends. *Polymer* 53, 4338–4343 (2012). DOI: 10.1016/j.polymer.2012.07.027.

60. García-Martínez J., Laguna O., Areso S., Collar E. P.: A dynamic – mechanical study of the role of succinil-fluoresceine grafted atactic polypropylene as interfacial modifier in polypropylene / talc composites. Effect of grafting degree. European Polymer Journal, 38, 1583–1589 (2002). DOI: 10.1016/S0014-3057(02)00051-4.

61. Wang J. J., Li Z. Z., Gu X. P., Feng L. F., Zhang C. L., Hu G. H.: A dissipative particle dynamics study on the compatibilizing process of immiscible polymer blends with graft copolymers. Polymer, 53, 4448–4454 (2012). DOI: 10.1016/j.polymer.2012.08.030.

62. Ramis X., Cadenato A., Morancho J. M., Salla J. M.: Polyurethane–unsaturated polyester interpenetrating polymer networks: Thermal and dynamic mechanical thermal behaviour. Polymer, 42, 9469–9479 (2001). DOI: 10.1016/S0032-3861(01)00492-X.

63. Chen C., Chen W., Chen M., Li Y.: Simultaneous full-interpenetrated polymer networks of blocked polyurethane and vinyl ester. Part I. Synthesis, swelling ratio, thermal properties and morphology. Polymer, 41, 7961-7967 (2000). DOI: 0032-3861/00/$.

64. Fan L., Hu C., Ying S.: Thermal analysis during the formation of polyurethane and vinyl ester resin interpenetrating polymer networks. Polymer, 37, 975-981 (1996). DOI: 0032-3861/96/$15.00+0.00.

65. Gryshchuk O., Jost N., Karger-Kocsis J.: Toughening of vinylester–urethane hybrid resins by functional liquid nitrile rubbers and hyperbranched polymers. Polymer, 43, 4763–4768 (2002). DOI: 10.1016/S0032-3861(02)00314-2.

66. Jost N., Karger-Kocsis J.: On the curing of a vinylester–urethane hybrid resin. Polymer, 43, 1383–1389 (2002). DOI: 10.1016/S0032-3861(01)00702-9.

67. Karger-Kocsis J., Fröhlich J., Gryshchuk O., Kautz H., Frey H., Mülhaupt R.: Synthesis of reactive hyperbranched and star-like polyethers and their use for toughening of vinylester–urethane hybrid resins. Polymer, 45, 1185–1195 (2004). DOI: 10.1016/j.polymer.2003.12.050.

68. Cho K., Lee D., Park C.: Effect of molecular weight between crosslinks on fracture behavior of diallylterephthalate resins. Polymer, 37, 813-817 (1996). DOI: 0032-3861/96/$15.00+0.00.

69. Janssen M., Zuidema J., Wanhill R. J. H.: Fracture Mechanics. Delft Academic Press/VSSD, Delft (2006).

70. ASTM D638: Standard Test method for tensile properties of plastics (2014).

71. Cateto C., Barreiro M., Rodrigues A.: Monitoring of lignin-based polyurethane synthesis by FTIR. Industrial Crops and Products, 27, 168-174 (2008). DOI: 10.1016/j.indcrop.2007.07.018.

72. Odian G.: Principles of Polymerization. Wiley-Interscience (2004).

73. Heatley F., Pratsitsilp Y., McHugh N., Watts D. C., Devlin H.: Determination of extent of reaction in dimethacrylate-based dental composites using solid-state ^{13}C m.a.s n.m.r spectroscopy and comparison with *FT*i.r. spectroscopy. Polymer, 36, 1859-1867 (1995). DOI: 10. 1016/0032-3861(95)90932-R

74. Podgórski M.: Structure-property relantionship in new phot-cured dimethacrylate-based dental resins. Dental materials*:* Official Publication of the Academy of Dental Materials, 28, 398-409 (2012). DOI: 10.1016/j.dental.2011.11.013.

75. Karger-Kcosis J., Gremmels J.: Use of Hygroghermal Decomposed Polyester-Urethane Waste for the Impact Modification of Epoxy Resins. Journal of Applied Polymer Science, 78, 1139-1151 (2000). DOI: 10.1002/1097-4628(20001031)78:5<1139::AID-APP240>3.0.CO;2-Q.

76. Liang Y., Pearson R.: Toughening mechanisms in epoxy-silica nanocomposites (ESNs). Polymer, 50, 4895-4905 (2009). DOI: 10.1016/j.polymer.2009.08.014.

77. Liu J., Sue H., Thompson Z., Bates F., Dettloff M., Jacob G., Verghese N., Pham H. Polymer, 50, 4683-4689 (2009). DOI: 10.1016/j.polymer.2009.05.006.

78. Sherman C., Zeigler R., Verghese N., Marks M.: Structure-property relationships of controlled epoxy networks with quantified levels of excess epoxy etherification. Polymer, 49, 1164-1172 (2008). DOI: 10.1016/j.polymer.2008.01.037.

79. Go, J A, and J F Mano. 2004. "Viscoelastic Behavior of Poly (Methyl Methacrylate) Networks with Different Cross-Linking Degrees:" 3735–3744.

80. Barua B., Saha M. C. 2011. "Tensile Stress Relaxation Behavior of Thermosetting Polyurethane Solid and Foams: Experimental and Model Prediction". Journal of Engineering Materials and Technology, 133. DOI: 10.1115/1.4004697.

81. Barry, Stephen E, and David S Soane. 1996. "Second Harmonic Generation in Carbon Dioxide Processed Thin Polymer Films" 9297 (96): 3565–3573.

82. Fancey K. S. 2005. "A Mechanical Model for Creep , Recovery and Stress Relaxation in Polymeric Materials" (2): 2–6. doi:10.1007/s10853-005-2020-x.

83. Akpa, Onoja M, and Emmanuel I Unuabonah. 2011. "Small-Sample Corrected Akaike Information Criterion : An Appropriate Statistical Tool for Ranking of Adsorption Isotherm Models." *DES* 272 (1-3): 20–26. doi:10.1016/j.desal.2010.12.057.

84. Spontak R. J., Vratsanos M. S. 2000. "Stress Relaxation Activation in Rubber-Modified Polymer Systems Exhibiting Controlled Miscibility through Blending". Macromolecules, 33, 2290-2292.

85. Pham, S. 1995. "Toughening of Vinyl Ester Resins with Modified Polybutadienes." *Polymer* 36 (17): 3279–3285. doi:10.1016/0032-3861(95)99426-U.

86. Fitzer E. 2012. "Carbon Fibres and Their Composites: Based on papers presented at the International Conference on Carbon Fibre Applications, San José dos Campos (SP), Brazil, 5-9 December 1983. Springer Science & Business Media, 2012.

87. Scott, Timothy F., Wayne D. Cook, and John S. Forsythe. 2002. "Kinetics and Network Structure of Thermally Cured Vinyl Ester Resins." *European Polymer Journal* 38: 705–716. doi:10.1016/S0014-3057(01)00244-0.

88. La Scala, John J., Joshua a. Orlicki, Cherise Winston, E. Jason Robinette, James M. Sands, and Giuseppe R. Palmese. 2005. “The Use of Bimodal Blends of Vinyl Ester Monomers to Improve Resin Processing and Toughen Polymer Properties.” *Polymer* 46 (9): 2908–2921. doi:10.1016/j.polymer.2005.02.011.

89. Liang, Guozheng, Ruilin Zuo, Tingli Lu, and Junlong Wang. 2005. “Modification of Vinyl Ester Resin by a New Thermoset Liquid Crystalline Diacrylate.” *Journal of Materials Science* 40 (8): 2089–2091. doi:10.1007/s10853-005-1242-2.

90. Robinette, E.J., S. Ziaee, and G.R. Palmese. 2004. “Toughening of Vinyl Ester Resin Using Butadiene-Acrylonitrile Rubber Modifiers.” *Polymer* 45 (18): 6143–6154. doi:10.1016/j.polymer.2004.07.003.

91. Chen, C.-H., W.-J. Chen, M.-H. Chen, and Y.-M. Li. 2000. “Simultaneous Full-Interpenetrating Polymer Networks of Blocked Polyurethane and Vinyl Ester Part I. Synthesis, Swelling Ratio, Thermal Properties and Morphology.” *Polymer* 41 (22): 7961–7967. doi:10.1016/S0032-3861(00)00173-7.

92. Fan, Lian Hua, Chun Pu Hu, and Sheng Kang Ying. 1996. “Thermal Analysis during the Formation of Polyurethane and Vinyl Ester Resin Interpenetrating Polymer Networks.” *Polymer* 37 (6): 975–981. doi:10.1016/0032-3861(96)87280-6.

93. Scott, Timothy F., Wayne D. Cook, and John S. Forsythe. 2008. “Effect of the Degree of Cure on the Viscoelastic Properties of Vinyl Ester Resins.” *European Polymer Journal* 44 (10): 3200–3212. doi:10.1016/j.eurpolymj.2008.07.009.